Chemical vapour deposition

Luzhao Sun[1,2], *Guowen Yuan*[3], *Libo Gao*[3]✉, *Jieun Yang*[4], *Manish Chhowalla*[4]✉, *Meysam Heydari Gharahcheshmeh*[5], *Karen K. Gleason*[5]✉, *Yong Seok Choi*[6,7,8], *Byung Hee Hong*[6,7,8]✉ *and Zhongfan Liu*[1,2]✉

Abstract | Chemical vapour deposition (CVD) is a powerful technology for producing high-quality solid thin films and coatings. Although widely used in modern industries, it is continuously being developed as it is adapted to new materials. Today, CVD synthesis is being pushed to new heights with the precise manufacturing of both inorganic thin films of 2D materials and high-purity polymeric thin films that can be conformally deposited on various substrates. In this Primer, an overview of the CVD technique, including instrument construction, process control, material characterization and reproducibility issues, is provided. By taking graphene, 2D transition metal dichalcogenides (TMDs) and polymeric thin films as typical examples, the best practices for experimentation involving substrate pretreatment, high-temperature growth and post-growth processes are presented. Recent advances and scaling-up challenges are also highlighted. By analysing current limitations and optimizations, we also provide insight into possible future directions for the method, including reactor design for high-throughput and low-temperature growth of thin films.

Chemical vapour deposition (CVD) is a widely used materials processing technology in which thin films are formed on a heated substrate via a chemical reaction of gas-phase precursors. In contrast to physical vapour deposition methods, such as evaporation and sputtering, CVD offers a clear advantage by relying on chemical reactions that enable tunable deposition rates as well as high-quality products with excellent conformality. The greater demand for semiconductor thin films starting after World War II was the initial driving force for rapid development of CVD technology[1–5]. Recently, low-dimensional materials such as carbon nanotubes, graphene and 2D transition metal dichalcogenides (TMDs) have injected new vitality into the electronics industry[6–8] and introduced more stringent requirements for successful CVD of these materials with high purity and fine structure. CVD allows the tuning of the structures and properties of the resulting products[9,10], and various advanced CVD systems and their variants have been developed, such as plasma-enhanced CVD[2] and metal–organic CVD (MOCVD)[4] (BOX 1). Usually, CVD does not require high-vacuum working environments, making it a popular technology for electronics, optoelectronics, surface modification and biomedical applications.

Irrespective of the variations in CVD types, the fundamental process is similar and consists of the following common elementary steps[11,12] (FIG. 1). First, the reactant gases are transported into the reactor. These reactant gases then either undergo gas-phase reactions to form intermediate reactants and gaseous by-products via homogeneous reactions or diffuse directly through the boundary layer to the substrate. In both cases, the reactant gases and the intermediate reactants adsorb onto the heated substrate surface and diffuse on the surface. The subsequent heterogeneous reactions at the gas–solid interface lead to continuous thin film formation via nucleation, growth and coalescence as well as formation of reaction by-products. Finally, any gaseous products and unreacted species desorb from the surface and are carried away from the reaction zone. The gas-phase reactions occur when the temperature is sufficiently high or additional energy is introduced, for example, in the form of plasma. In addition, the heterogeneous reaction is essential if the deposition reaction relies on the surface catalysis of the underlying substrate, such as in the case of the catalytic growth of graphene on a metal surface.

In this Primer, we first provide an overview of the CVD instrumentation set-up before describing best practices for material preparation and characterization. The growth of graphene on metal and dielectric substrates are taken as representative examples of catalytic CVD and non-catalytic CVD processes, respectively. We then demonstrate the flexibility of this method by discussing important applications of CVD, including growth of binary and ternary 2D materials and polymeric thin films. We also highlight recent progress and challenges when scaling-up this technology, an important aspect of CVD when applied to industry. Finally, we discuss what affects experimental reproducibility, the current limitations of the technique and future

✉*e-mail:* *lbgao@nju.edu.cn*; *mc209@cam.ac.uk*; *kkgleasn@mit.edu*; *byunghee@snu.ac.kr*; *zfliu@pku.edu.cn*

https://doi.org/10.1038/s43586-020-00005-y

Author addresses

[1]Center for Nanochemistry, Beijing Science and Engineering Center for Nanocarbons, Beijing National Laboratory for Molecular Sciences, College of Chemistry and Molecular Engineering, Peking University, Beijing, China.
[2]Beijing Graphene Institute, Beijing, China.
[3]National Laboratory of Solid State Microstructures, School of Physics, Collaborative Innovation Center of Advanced Microstructures, Nanjing University, Nanjing, China.
[4]Department of Materials Science and Metallurgy, University of Cambridge, Cambridge, UK.
[5]Department of Chemical Engineering, Massachusetts Institute of Technology, Cambridge, MA, USA.
[6]Graphene Research Center, Advanced Institute of Convergence Technology, Suwon, Korea.
[7]Department of Chemistry, Seoul National University, Seoul, Korea.
[8]Graphene Square Inc., Suwon, Korea.

developments of CVD together with exploration of new materials.

Experimentation

To obtain high-quality thin films by CVD, suitable equipment is needed, and custom-built systems provide the flexibility of operation often desired by CVD researchers. In this section, we discuss a series of designs that satisfy the requirements of materials synthesis, including the heating methods, gas-flow control, the loading of substrate and so on. In addition, the growth parameters, including substrate, temperature, atmosphere, pressure and so on, are essential for controlling the quality of as-grown materials as well as the reaction rate (growth rate). Here, we will introduce CVD growth of graphene following the procedure of substrate pretreatment, heating, annealing, high-temperature growth and cooling.

CVD equipment

A CVD system must meet the following basic requirements: delivery of the gas-phase reactants in a controllable manner; provision of a sealed reaction chamber; evacuation of the gases and control of the reaction pressure; supply of the energy source for the chemical reactions; treatment of the exhaust gases to obtain safe and harmless levels; and automatic process control to improve the stability of the deposition process. FIGURE 2 shows a typical CVD system consisting of a gas delivery system, a reaction chamber, a vacuum system, an energy system, an exhaust gas treatment system and an automatic control system.

Gas delivery system. Safety and process control are two of the key aspects of this design, especially considering the possibility of using high-pressure, toxic, flammable and explosive gas, liquid or solid precursors. The gaseous reactants are usually stored in high-pressure gas bottles placed in cool places outdoors or in cabinets at a constant negative pressure, to ensure safety. The gas supply line starts at the outlets of the high-pressure gas bottles, which are fitted with mechanical pressure regulators to control the pressure, and ends at the inlet of the reaction chamber. Valves (for example, ball shut off, needle shut off and pneumatic valves) and metal gasket seal connectors are often used to ensure a good sealing performance.

Mass flow controllers are essential for the gas supply, where the gas flow rate is automatically set via feedback control according to the mass of flowing gas. Liquid source reactants are delivered by 'bubbling' a carrier gas controlled by the mass flow controller[13,14] (FIG. 2b). Solid source precursors that are less volatile are introduced to the reaction chamber by dissolution in a suitable solvent[15] or by sublimation into the gas phase[16–22].

Reaction chamber. The horizontal[23,24] (FIG. 2a) and vertical[25,26] (FIG. 2c–e) configurations are the two main configurations of the reaction chamber (BOX 1). The reaction chamber itself is usually a quartz tube, widely employed in semiconductor manufacturing because of its tolerance to high temperatures and to rapid heating and cooling. A gas inlet injector is connected to the chamber using a metal flange, which is fitted with cooling components. To guarantee that the gas flow is laminar, a gas distributor with through-holes is usually employed[23,25] (FIG. 2c–e). The substrate is usually located on a substrate holder (also known as a 'boat' or 'susceptor') composed of quartz or graphite because of their good chemical stability and high-temperature resistance[23,27,28]. In order to meet the target deposition characteristics (thickness, composition and so on),the configuration of the substrate holder and the deposition conditions (total gas flow, gas composition, temperature, pressure and so on) must be optimized via experimental and numerical process engineering studies[23,25,26,29,30]. In manufacturing applications, a cooling chamber with a loading/unloading subsystem is necessary to improve the productivity.

Vacuum system. Purging the deposition chamber to start the deposition process and obtaining the necessary pressure for transport of the reactants relies on the vacuum system, where measurement and control of the vacuum are essential and complement one another. To measure the pressure of the vacuum system, various gauges are alternated: the Bourdon gauge, piezo sensor, capacitance manometer and diaphragm manometer are the main mechanical gauges, which can measure the vacuum by detecting physical changes in the strain or electrical capacitance, for example. The Bourdon gauge is inexpensive and has a long life, but it does not have an electronic output, and so is not suitable for feedback control (FIG. 2f). Using a capacitance manometer, a measurement range of four orders of magnitude can be achieved for almost any gas, and the signal can be transported to an electronic display or a feedback controller (FIG. 2g). The diaphragm manometer operates in the same way as the capacitance manometer, only with a smaller range of measurement. In addition, gas property gauges, such as thermocouple gauges and the Pirani gauge, are inherently inaccurate, as their value is determined by the types of gases and temperatures; however, when calibrated, they can be used to measure certain conditions. Furthermore, ionization gauges are commonly employed under high or ultra-high vacuum conditions.

To control the pressure, the use of a throttle valve or a needle valve is effective, and the downstream flow rate can be controlled by adjusting the opening degree of the valve gate[31]. The chamber pressure will then stabilize

Box 1 | **CVD categories and variants**

Horizontal chemical vapour deposition (CVD) and vertical CVD are based on the reactor configurations or the directions of gas flow. The horizontal tube reactor is the most common configuration, where the substrates are mounted horizontally, vertically or with a tilt angle to adjust the gas flow. The vertical reactor is usually equipped with a showerhead mixer, which is beneficial for material uniformity and growth rate.

Low-pressure CVD and atmospheric pressure CVD are based on the working pressure. In low-pressure CVD, a vacuum pump drives the gas flow. By contrast, atmospheric pressure CVD usually does not require a pump and results in a slow flow rate for the reactive gas.

Hot-wall CVD and cold-wall CVD refer to the heating methods of thermal CVD. In hot-wall CVD, the entire reaction chamber is heated by an external furnace with a uniform temperature. In cold-wall CVD, only the substrate and its vicinity are heated, and the reactor wall is cold, allowing for rapid heating and cooling. Resistance heating, hot plates and induction heating methods are common for cold-wall CVD.

Plasma-enhanced CVD, photo-assisted CVD and laser-assisted CVD are variants of thermal CVD involving additional components and the introduction of other types of energy to promote the CVD reaction. In plasma-enhanced CVD, plasma — a partially ionized high-energy gas — is generated by direct current, radio-frequency voltage or microwave sources and coupled to the reactor, resulting in a major drop of the reaction temperature. In photo-assisted/laser-assisted CVD, light from a high-intensity lamp or laser is used to promote the deposition.

Metal–organic CVD (MOCVD) utilizes metal–organic precursors (usually volatile toxic liquids) that are vaporized to form thin films. MOCVD is widely used to synthesize III–V compound semiconductors (made of elements from groups III and V in the periodic table) for optoelectronics.

Hot filament/wire CVD utilizes resistively heated filaments (wires) suspended above a substrate held at a lower temperature. The filaments cause thermal decomposition, leading to precursors that then adsorb onto the cooler substrates. A refractory metal such as tungsten, tantalum or molybdenum is commonly used as the filament material. Typically, inorganic films such as amorphous silicon or silicon nitride are deposited.

Initiated CVD is a form of hot filament/wire CVD for growing electrically insulating polymer thin films. The initiated CVD method utilizes an initiator and monomers as vapour-phase reactants, which absorb and undergo chain-growth polymerization on the cooled substrate. The use of the initiator enables much lower filament temperatures, which preserves the organic functional groups of the monomer. Incorporating the functional groups allows control over the wettability and surface reactivity.

Oxidative CVD utilizes oxidant and monomer vapours, which undergo spontaneous reaction upon adsorption to the substrate. Oxidative CVD produces step-growth polymerization and, typically, results in conducting and semiconducting polymer films.

Atomic layer deposition and molecular layer deposition are two similar variants of CVD for depositing inorganic and organic thin films, respectively. For atomic and molecular layer deposition processes, precursors are introduced sequentially. Self-limiting absorption and surface reactions of the precursors results in layer by layer growth of high-quality thin films. Between layers, the remaining precursor is purged out by the carrier gas.

when the flow rate of the incoming gas is equal to that of the exhaust, which can be automatically or manually controlled by real-time pressure monitoring[31].

Pumps provide the driving force for the vacuum and mass transport within the system. For a CVD system, mechanical pumps are adequate for many operations and can provide a vacuum of 1 Pa. Oil pumps are cheaper than dry pumps of the same power, but bring additional contaminants into the system. If the reaction chamber is large, a rotary pump (pumping speed ranging from 0.5 to 325 l s^{-1}) with a Roots pump (50–35,000 l s^{-1}) is a good choice for a fast exhaust. Finally, a vacuum isolation valve (also known as a block valve) is used between the outlet of the CVD chamber and the pump to shut off the pumping process.

Energy system. For a thermal CVD process, the heating components, thermal insulation structure and temperature measuring elements are important. FIGURE 2a shows a common resistance heating furnace, which consists of three heating zones and aluminium silicate insulating cotton to ensure a uniform temperature field over a sufficient length. Thermocouples, which are the most common temperature measuring device, are placed between the quartz tube and the heating components, and are connected to a proportional–integral–derivative regulator. Several types of thermocouples exist (including B, K, R and S), which are suitable for application under different conditions[32]. In the case of a large reactor (diameter >25 cm), the inclusion of thermocouples inside the chamber is necessary to calibrate the temperature. Cold-wall reactors most frequently use a graphite heater that introduces an electrical current into the chamber[29,33], and a pyrometer is commonly employed to measure the temperature. Plasma can also be used to provide energy by electrical discharge of the gaseous media; in this case, the electron temperatures are significantly higher than the neutral and ion temperatures[34,35]. As an example, an inductively-coupled plasma source is illustrated in FIG. 2a, and this can be placed against part of the reaction chamber for facile integration into the tube reactor. The geometry and materials of the substrate holder also influence the heat transfer, and radiant heating with a halide lamp[36], electric induction[37] or laser can be used to specifically heat the substrate.

Exhaust gas treatment system. The by-products and unreacted chemical substances of CVD tend to be flammable, toxic or harmful to the pumps, and therefore must be safely treated. This is usually done with either one or a combination of components such as cold traps, chemical traps, particle traps, wet scrubbers and vents[15,19]. A cold trap is used to condense volatile gases and cool exhaust gases to stop the temperature of the vacuum pump oil from increasing. In addition, various corrosive gases can be reacted or adsorbed by passing through a chemical trap, and a particle trap can provide protection against pump wear. To further convert the exhaust into harmless substances, a burning component or a wet scrubber can also be employed[32].

Experimental methods for materials growth

Here, we introduce the materials preparation process using graphene as an example (FIG. 3). Graphene is a nanomaterial consisting of single-layer sp^2 bonded carbon atoms that is challenging to synthesize in a controllable manner. The introduction of catalytic metal substrate paved the way for growing high-quality monolayer graphene films by following a self-limited growth mode. In the case of growing on a non-catalytic insulating substrate, a higher temperature or additional energy supply is needed to promote decomposition of the precursors.

Substrate pretreatment. Selecting an appropriate substrate is essential for CVD growth because different substrate catalytic abilities and carbon solubilities result in different graphene growth modes. Transition metals (for example, copper and nickel)[38,39] and insulating substrates

(for example, SiO_2, Al_2O_3 and glass)[40–42] are typical substrates on which the heterogeneous catalytic reaction and the gas-phase reaction dominate the growth processes, respectively. To grow high-quality graphene, cleaning of the substrate is necessary. Electrochemical polishing, for example on copper foil, can be employed to reduce the level of contaminants and decrease the surface roughness (FIG. 3a). As for silicon wafers or sapphire wafers, typical cleaning procedures employed in the semiconductor community (such as picking) are applicable (FIG. 3e).

Heating and annealing. After loading the substrate onto the substrate holder and transporting it to the desired location in the CVD chamber, the gate is closed and the chamber is checked for any air leakage. The substrate is then heated to 1,000 °C and annealed under a non-reactive atmosphere (FIG. 3b). During this procedure, the introduction of very small quantities of oxygen into the chamber can aid in reducing the nucleation density of graphene by burning any carbon-containing contaminants[43,44] that could seed graphene during the growth process. Hydrogen is commonly introduced to reduce and activate the weakly oxidized copper surface. In addition, a temperature gradient is beneficial for preparing a single-crystal metal substrate to promote subsequent graphene growth[28,45–47] (FIG. 3b).

High-temperature growth. Graphene growth is initiated by introducing a hydrocarbon precursor (methane is most commonly used) that decomposes into active carbon species to fuel the growth of graphene. If the substrate is a metal with a relatively high catalytic ability and a low carbon solubility, such as copper, the hydrocarbon precursors are initially adsorbed onto the substrate prior to step-by-step decomposition into active carbon species under the form of CH_x ($x = 3, 2, 1, 0$)[48]. Subsequent growth takes place through nucleation, growth and coalescence of the graphene seeds to produce a continuous film[49,50] (FIG. 3c). During the nucleation stage, the nucleation density and orientation of the nuclei determining the domain size of the graphene film are influenced by temperature, the concentration of active carbon species, the surface properties of substrate and so on. In the surface catalysis-dominated process, the formed graphene islands continuously expand until they merge into a film: this is called the self-limited growth mode. Research on the growth kinetics of this self-limited mode is essential to increase the growth rate and improve the graphene quality. According to the Arrhenius equation $k = Ae^{\frac{-E_a}{RT}}$, the growth rate k is exponential with $-E_a/RT$, where E_a is the growth activation energy, T is temperature and R is the universal gas constant. Various strategies are effective at increasing the growth rate and include introducing surface oxygen, employing metals with high catalytic activity or increasing the temperature and concentration of the precursors. The gas-phase reaction when catalysed on the surface of the metallic substrate can produce significant amounts of by-products and induce the formation of amorphous carbon contaminants[21,51], which is often overlooked.

For non-metallic substrates (for example, SiO_2 or Al_2O_3), if the precursor concentration and temperature are both sufficiently high then the thermally decomposed active carbon species can deposit onto the substrate and form a graphene film[30,40,41,52] (FIG. 3f), where gas-phase decomposition reactions play a crucial role. In this case, employing high-energy plasma can promote the decomposition of the carbon precursor and lower the growth temperature (<600 °C)[34]. However, due to a lack of catalytic activity from the substrate and a reaction temperature below the graphitization temperature, the quality of the graphene grown using this set-up is poor compared with graphene grown on a copper surface[9,42].

Cooling. The cooling process also contributes to the growth of graphene. If the substrate is a metal with a high carbon solubility, such as nickel, the carbon dissolved in the bulk nickel will segregate and form

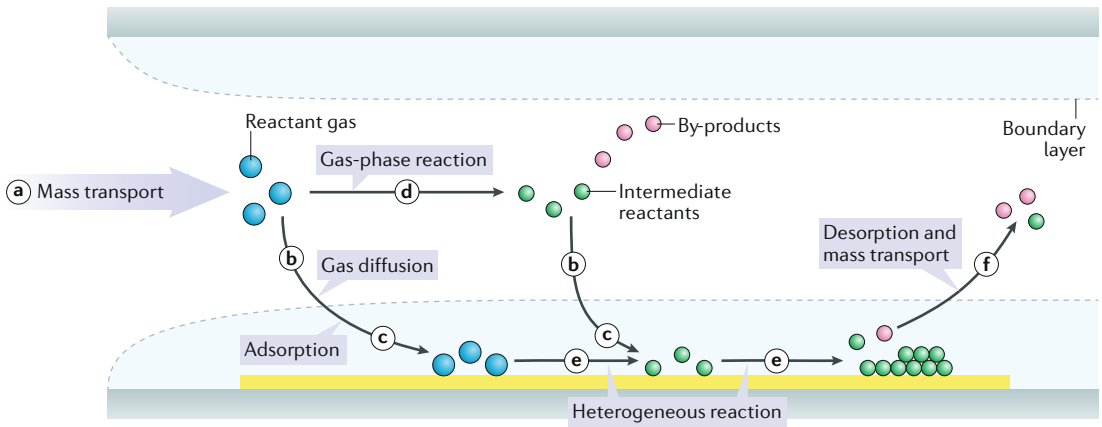

Fig. 1 | **Schematic of general elementary steps of a typical CVD process.** First, reactant gases (blue circles) are transported into the reactor (step a). Then, there are two possible routes for the reactant gases: directly diffusing through the boundary layer (step b) and adsorbing onto the substrate (step c); or forming intermediate reactants (green circles) and by-products (red circles) via the gas-phase reaction (step d) and being deposited onto the substrate by diffusion (step b) and adsorption (step c). Surface diffusion and heterogeneous reactions (step e) take place on the surface of substrate before the formation of thin films or coatings. Finally, by-products and unreacted species are desorbed from the surface and forced out of the reactor as exhausts (step f). CVD, chemical vapour deposition.

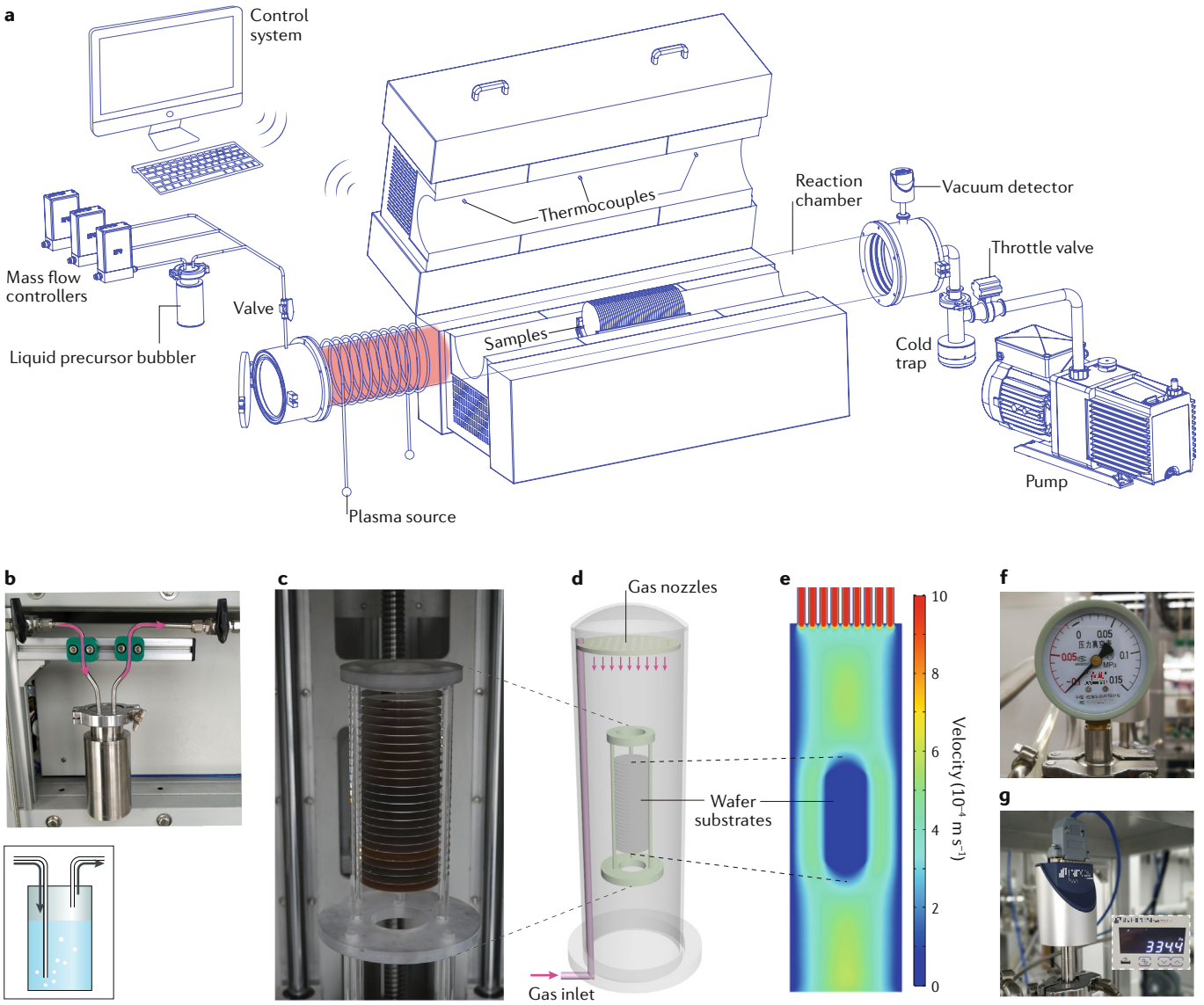

Fig. 2 | **Typical CVD equipment. a** | Schematic diagram of a typical horizontal chemical vapour deposition (CVD) system, which includes a gas delivery system, the quartz reaction chamber, a vacuum system, the energy system and an auto-control system. **b** | A liquid precursor bubbler, which can also be used to provide solid precursors by dissolution in a suitable solvent. **c**–**g** | A vertical reactor for scalable growth of graphene wafers, where the 25 wafers can be loaded on the quartz substrate holder (part **c**). The multiple gas inlet nozzles are designed (part **d**) to improve the uniformity of gas flow, which is simulated based on the finite element method[25] (part **e**). The Bourdon gauge (part **f**) and capacitance manometer (part **g**), which are commonly used to measure the pressure of the vacuum system. Parts **c**–**e** adapted with permission from REF.[25], Elsevier.

few-layer graphene sheets[12,53]. Through designing a synergistic binary alloy (such as Cu/Ni, Ni/Mo, Co/Mo) as a substrate and controlling the cooling rate, the number of graphene layers that form can be controlled during the segregation process[54–56] (FIG. 3d). The thermal expansion mismatch between graphene and its underlying substrate will result in step bunches and wrinkles (including standing collapsed wrinkle and folded wrinkle) during cooling[57–61] (FIG. 3g). The carbon solubility[62] at 1,000 °C and thermal expansion[63] of typical substrates are presented in TABLE 1.

Finally, fast cooling, which is achieved either by moving the samples out of the hot zone or by moving the furnace, is commonly employed to increase production efficiency[9,64]. A programmable cooling procedure can also be used to achieve a desired structure in the produced materials[64,65]. As a rule of thumb, the flow rates of reactant gases (such as hydrogen and methane) are usually maintained during the cooling process to protect the as-formed graphene film from etching by oxygen leaked from the atmosphere. After the temperature drops below 100 °C, the furnace chamber gate can be opened and the samples can be unloaded from the substrate holder.

Results

CVD is directly related to some of the properties of the as-grown materials. In order to assess the CVD method, the as-grown materials must be characterized in-depth to

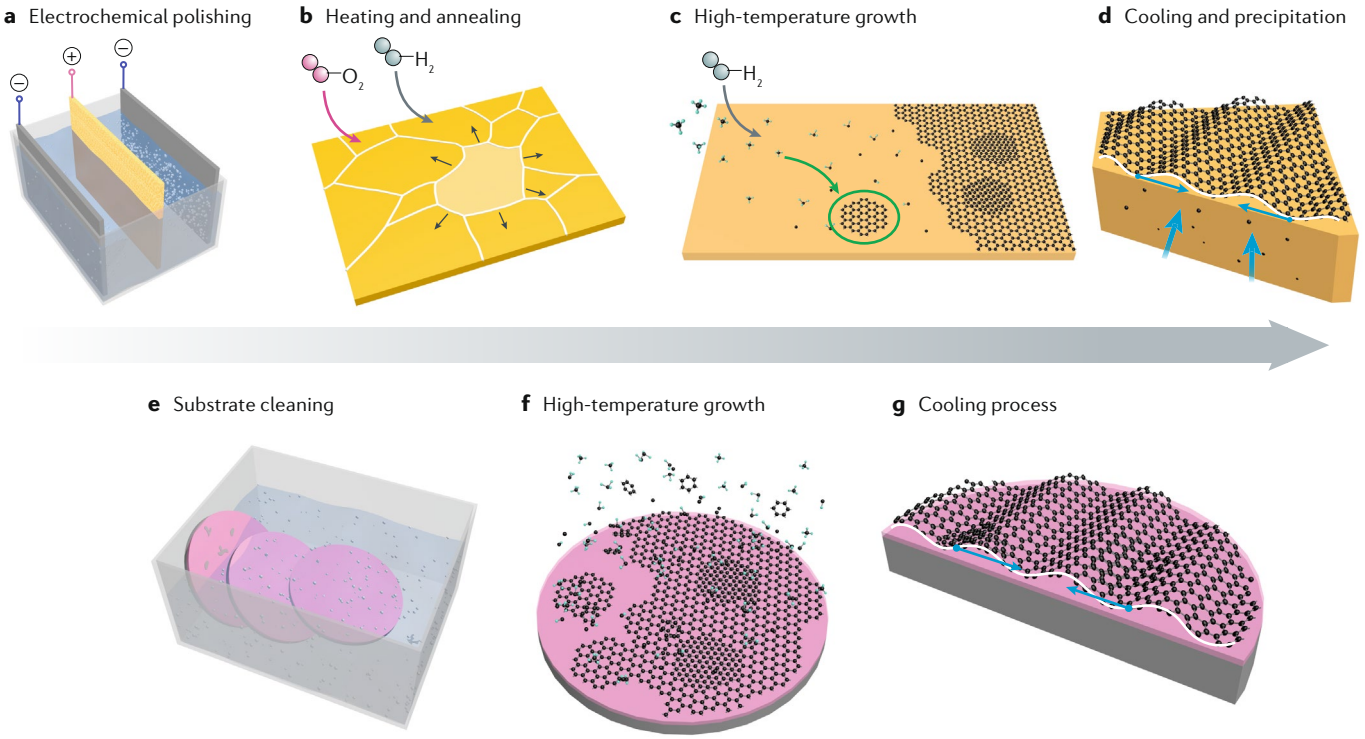

Fig. 3 | **Schematic of experimental processes for growing graphene. a–d** | Processes of growing graphene on metal substrates: electrochemical polishing for cleaning and smoothing the substrate (part **a**); heating and annealing to reduce the nucleation sites and enlarge the grain size of metal substrate (part **b**); high-temperature growth, which is dominated by the surface reaction (part **c**); and precipitation and crumpling during the cooling process (part **d**). **e–g** | Processes of growing graphene on dielectric substrates: cleaning the dielectric substrate (part **e**); gas-phase reaction dominated growth at high temperature (part **f**); and thermal contraction induced crumpling during the cooling process (part **g**).

obtain morphological and structural information. Using the CVD growth of graphene as an example, we describe numerous characterization methods to assess the macroscopic quality, atomic structure, electronic structure and purity of the resulting graphene (TABLE 2). A transfer process of the as-grown graphene from the metal catalytic substrate to a target substrate is usually necessary when assessing graphene quality because an appropriate substrate is important for some characterization techniques.

Assessing morphology of materials

Optical microscopy[9] is a simple and quick tool to identify the macroscopic morphology of graphene. Its lower resolution yields information such as the location of graphene on the substrate, the number of graphene layers and their shape, and so on. Optical microscopy is widely used for exfoliated graphene on SiO_2/silicon, but is only effective on some silicon substrates with a specific oxide thickness such as 90 or 280 nm (REF.[66]). For CVD-grown graphene on metal substrates such as copper, nickel, platinum, ruthenium and so on, the graphene usually first needs to be transferred onto these SiO_2/silicon substrates for optical microscopy observation[67–69] (FIG. 4a). However, for the case of graphene grown on copper, selectively oxidizing the graphene/copper interface can cause the oxidized copper to act as a specific substrate[70–72] and reveal the graphene individual domain shapes, surface coverage, layer numbers or grain boundaries. Graphene domains are delineated by grain boundaries; thus, increasing the crystal size of the substrate as well as bonding uniformly-oriented grains seamlessly will help minimize the concentration of grain boundaries. In addition, the multifunction optical microscopy modes of dark-field or polarized light can also increase the image contrast[73].

Scanning electron microscopy is another popular tool to characterize the morphology of graphene, as it provides nanoscale spatial resolution and greater depth of field than optical microscopy. It utilizes the attenuation effect of graphene layers on secondary electrons emitted from the underlying substrate[7,70,74,75]. Normally, in scanning electron microscopy images, a graphene-covered region is darker than the bare substrate (including metal and SiO_2/silicon). The colour of these regions darkens as the number of graphene layers increases, which is beneficial for distinguishing the layer number of graphene[43,76] (FIG. 4b). The side-attached Everhart–Thornley detector is most frequently used, which allows high-contrast images at low acceleration voltage ($V_{acc} \leq 5$ kV). The electron energy and density of the electron beam should be carefully set according to the conductivity of the substrate because the electron beam will inevitably break atomic lattices in graphene.

Atomic force microscopy is an important method to measure surface morphology at a subnanometre-scale resolution[7,39,69], and its multifunctions can also measure mechanical, electrical and magnetic properties[77].

Domain
A region of a single crystal that is delineated by grain boundaries or the edges of an isolated island.

Raman scattering
An inelastic scattering of photons by matter, by which the energy of the incident photon is changed.

Atomic force microscopy scans a sharp tip over a sample surface without electron or photon interactions. The surface roughness, thickness, cleanliness, wrinkles, domain sizes and shapes as well as the bonding status of CVD-grown graphene can all be obtained by this technique[51,78–80] (FIG. 4c,d) for both graphene on its original substrate and graphene transferred on an insulating substrate. Owing to the van der Waals interactions between graphene and the underlying substrate, the thickness of monolayer graphene is usually between 0.6 and 1.5 nm, which is much larger than graphene's interlayer spacing of 0.34 nm.

Assessing atomic structure

CVD-grown graphene can be affected by adsorbed atoms and molecules, and display distorted lattices, grain edges or grain boundaries, so it is important to analyse its atomic structure. Similar in operation to atomic force microscopy, scanning tunnelling microscopy (STM) is another proximal probe imaging technology based on the quantum tunnelling effect. It has very high spatial resolution because of the exponential relationship between the tunnelling current and the distance between the conducting surface and the sharp scanning tip, which means the honeycomb lattice of graphene or its morphology over hundreds of nanometres with atomic resolution can be easily acquired[81]. Being a surface-sensitive technique, STM characterization requires that the graphene is on a conductive and ultra-smooth substrate. STM images clearly present the point defects, atomic structures of grain boundaries or the edges of graphene[81–83], with zigzag edges preferred in CVD-grown graphene grains on various metals[81,84–86] (FIG. 4e). STM also confirms that CVD-grown graphene films retain continuous atomic lattices over metal steps and perfect lateral heterostructure between graphene and hexagonal boron nitride (h-BN)[87–90] (FIG. 4f). The strong coupling between graphene and the growth substrate often gives rise to Moiré patterns (FIG. 4g), and these superstructures vary with their twist angles and the strength of their interactions[58,91–93].

Table 1 | **Carbon solubility and thermal expansion properties of CVD substrates**[62,63]

Substrate	Carbon solubility at 1,000 °C (at.%)[63]	Coefficient of thermal expansion (10^{-6} K^{-1})[64]
Graphene	–	–7
Copper	0.04	16.7
Nickel	1.3	12.8
Platinum	1.76	8.9
Cobalt	3.41	13.7
Ruthenium	1.56	6.7
Palladium	5.98	11.6
Iridium	1.35	6.5
SiC	–	3.5
Silicon	–	2.5
Quartz (SiO_2)	–	0.4
Sapphire (Al_2O_3)	–	5.0–5.6

CVD, chemical vapour deposition.

Transmission electron microscopy is a technique commonly used to image the atomic structures of lattices, strains, defects and grain boundaries[94–97] of materials, including graphene and other 2D materials. It has very high resolution, with a recently demonstrated lateral resolution lower than 0.1 nm (REF.[98]). Samples for transmission electron microscopy imaging must be suspended or supported on an ultra-thin film, so designed micro-grids with through-holes or a carbon membrane are usually employed. If the transmission electron microscope is fitted with an aberration corrector, the operation voltage can be reduced and a subnanometre-scale resolution can be achieved. By using an aberration-corrected annular dark-field scanning transmission electron microscope, graphene's grain boundary structures with distorted pentagonal, heptagonal and octagonal rings have been observed[95] (FIG. 4h).

In addition to the above techniques, electron backscatter diffraction[46], X-ray diffraction[99], selected area electron diffraction[100] and low-energy electron diffraction[97] are also used to characterize CVD-grown graphene. Electron backscatter diffraction and X-ray diffraction are usually used to measure the crystalline orientation of the growth substrate, such as Cu(111), Pt(100), Ru(0001) and so on. Selected area electron diffraction implemented in a transmission electron microscope is usually used to confirm the crystalline orientation of graphene, and the selected area electron diffraction pattern can be used to calibrate the lattice constant of graphene. The measurement conditions of low-energy electron diffraction require an ultra-high vacuum and an ultra-smooth surface, and its reduced operation voltage is safer for most 2D materials.

Assessing electronic structure

Spectroscopic techniques can provide information regarding the bonding status, electronic structures and purity of CVD graphene through the interactions between atomic lattices and photons with different energies.

Graphene was characterized early on using Raman spectroscopy[101,102], which relies on Raman scattering and provides information about lattice vibrations (that is, phonons) in materials. Similar to exfoliated graphene on SiO_2/silicon, the Raman spectrum of CVD-grown graphene mainly consists of four vibration modes[101]: a layer-dependent C peak (29–44 cm^{-1}), a defect-dependent D peak (1,340–1,380 cm^{-1}), a hexagonal lattice-dependent G peak (1,550–1,620 cm^{-1}) and a 2D peak from a two-phonon process (2,650–2,760 cm^{-1}). All of the above values are collected using a laser wavenumber of 532 nm. By fitting the experimental data with a Lorentzian function, the position, shape, full width at half maximum and relative intensity of the Raman peaks can be obtained, from which information such as the layer number, defects, strain and doping level of CVD-grown graphene can be extracted[68,103,104] (FIG. 4i,j) for both graphene on metals and graphene transferred on other substrates. As an example, during CVD of graphene on metal, the metal substrate and the high temperature will introduce doping and strain in the graphene: this is easily characterized by the shift and relative intensity ratio of the G peak and the 2D peak compared with graphene's intrinsic

status[79,91] (that is, when it is in its suspended exfoliated initial state). In addition, CVD-grown graphene usually has point defects, grain boundaries or wrinkles, all of which contribute to the D peak[105,106] (FIG. 4j).

CVD graphene usually couples with the metal substrates, which alters its electronic structure significantly and causes it to exhibit p-type or n-type doping, an opened band gap and so on[107]. These effects can be detected by angular resolution photoemission spectroscopy[108] and scanning tunnelling spectroscopy[91]. The Dirac core of graphene in its intrinsic state is located at the Fermi level, whereas the position of the Dirac point for CVD graphene on metals usually shifts because of the charge transfer to or from the growth substrates[107–109]. For example, the Dirac point for monolayer graphene grown on copper is usually found at –450 to –300 meV with n-type doping and a band gap of 50–350 meV (REF.[110]) (FIG. 4k). In contrast to the large scanning area of angular resolution photoemission spectroscopy, scanning tunnelling spectroscopy detects the electronic structure at atomic resolution. Similarly to STM, it requires graphene to have a conductive and smooth substrate, and can measure the doping type, band gap and density of states at the atomic scale[91] (FIG. 4l).

For heterogeneous doping in CVD-grown graphene, X-ray photoelectron spectroscopy, energy-disperse spectroscopy and electron energy loss spectroscopy yield the binding energy, element species and relative elemental ratio[111]. With energy-disperse spectroscopy or electron energy loss spectroscopy equipped to a transmission electron microscope, the element distribution can also be imaged at atomic resolution.

Applications

In addition to graphene, 2D materials consisting of two or more elements, such as TMDs, h-BN, Mo_2C, Bi_2O_2Se and so on, and polymeric thin films can also be successfully synthesized by CVD. In contrast to growing

Table 2 | **Characterization tools and their settings for assessing graphene quality and structure**

Assessment tool	Spatial resolution	Property	Advantages	Disadvantages	Considerations
Optical microscopy	Micrometres or less	Individual domain shapes; surface coverage; number of layers; grain boundaries; defects (wrinkles and folds)	Simple to operate; large-area characterization; non-destructive to the sample	Low resolution; usually needs a suitable substrate	Clearer images when choosing a suitable wavelength of light or adding an optical filter
Scanning electron microscopy	Approximately nanometres	Individual domain shapes; surface coverage; number of layers; grain boundaries; defects (wrinkles and folds)	Simple to operate; large-area characterization; high resolution; good environmental adaptability	Damages the graphene atomic lattice	Based on electron scattering; electron beam energy ranges from a few 100 eV to a few keV
Atomic force microscopy	Nanometres or less	Individual domain shapes; surface coverage; roughness; grain boundaries; number of layers	High resolution; good environmental adaptability	Scanned area is small; scanning speed is slow; unsuitable for samples with significant surface topography	Sample surface must be clean; pollutants contaminate the tip and can result in virtual and/or false images
Scanning tunnelling microscopy	Ångstroms or less	Atomic structures (point defects, grain boundaries); crystal orientation	Atomic resolution; non-destructive	Scanned area is small; substrate must be conductive and ultra-smooth; complex and expensive	Based on quantum tunnelling effect; two possible operation modes (constant current or constant height)
Transmission electron microscopy	Ångstroms or less	Atomic structures (point defects, grain boundaries); crystal orientation; purity	Atomic resolution; can obtain cross-section geometry	As-grown graphene must be transferred to a suitable substrate	High-energy electron beam (several 10 keV to few 100 keV) can induce defects
Raman spectroscopy	~100 nm (diffraction limit)	Number of layers; defects; strain; doping	Simple to operate; high sensitivity; spatially resolved distribution easily obtained by mapping the sample	Qualitative only	SiO_2 is the most frequently used substrate
X-ray photoelectron spectroscopy	100 µm	Purity	Surface-sensitive technique to analyse elemental composition and chemical state	Low spatial resolution; no accurate quantification	Detecting depth ranges from 1 to 10 nm
Angular resolution photoemission spectroscopy	Approximately millielectronvolts (relies on the resolution of the analyser, the sample and the ultraviolet source)	Electronic properties (band structure); doping	Band structure can be directly observed; as-grown graphene can be directly characterized	Band structure above the Fermi surface cannot be obtained; complex and expensive	Based on the photoelectric effect

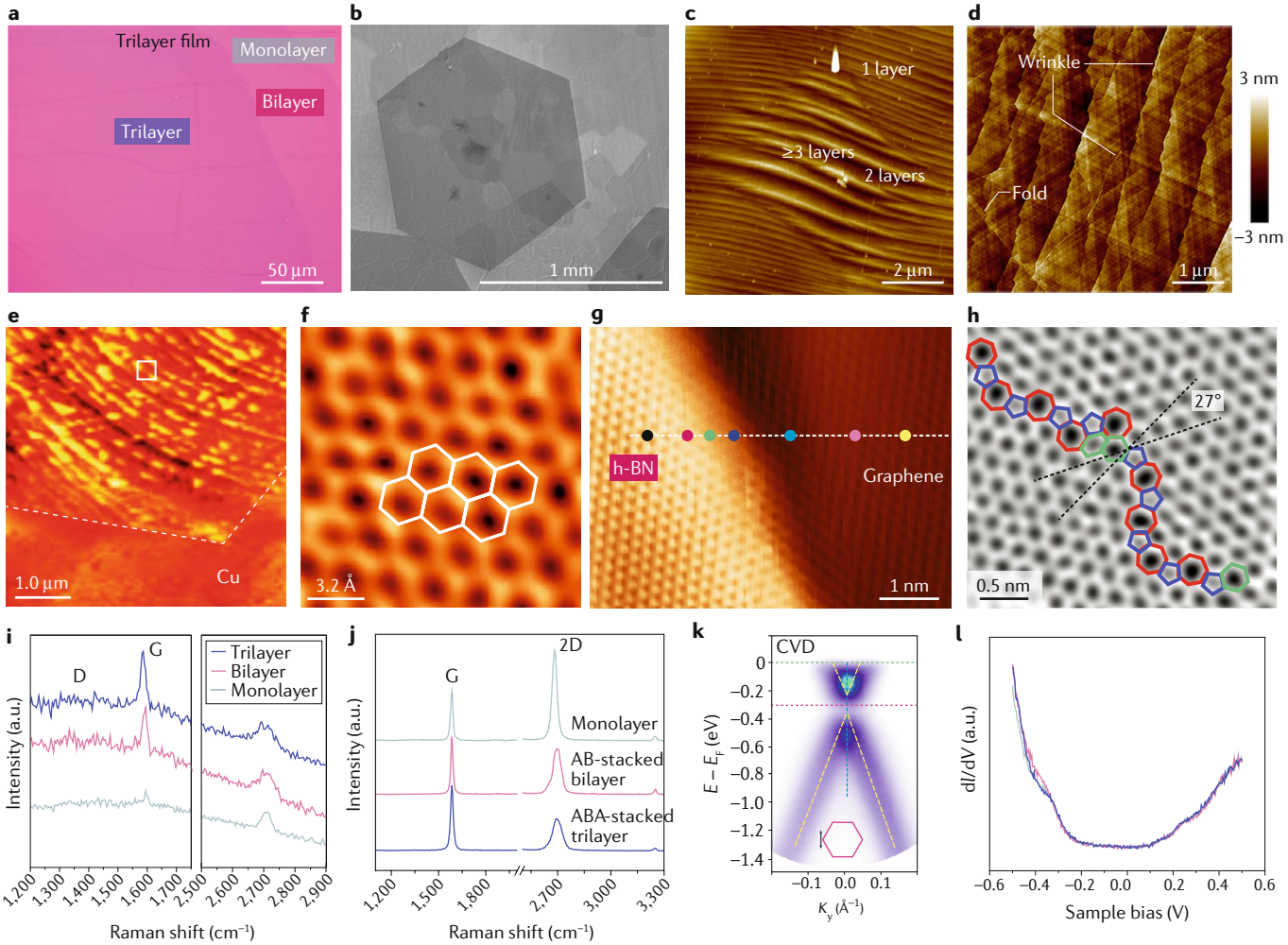

Fig. 4 | **Characterization of CVD-grown graphene. a** | Optical microscopy image of the transferred film on SiO_2/silicon substrate; the layer number can be distinguished by the colour contrast[68]. **b** | Scanning electron microscopy image of graphene domains grown on platinum foil; copper surface roughing changes with the number of graphene layers[69]. **c** | Typical atomic force microscopy (AFM) image of graphene grown on copper foil[79]. **d** | AFM image of graphene grown on Cu(111), where there are some wrinkles and folds[91]. **e** | Scanning tunnelling microscopy (STM) image (sample bias −2 V, tunnelling current 50 pA) near a corner of a hexagonal graphene grain on copper foil. **f** | Atomic-resolution STM image[81] corresponding to the white square in part **e**. **g** | Graphene–hexagonal boron nitride (h-BN) boundary structure imaged by atomic-resolution STM[90]. **h** | Atomic-resolution transmission electron microscopy image of the typical grain boundary in chemical vapour deposition (CVD)-grown graphene film[95]. **i** | Typical Raman spectra of CVD graphene on copper[79]. **j** | Raman spectra of monolayer, AB-stacked bilayer and ABA-stacked trilayer graphene transferred onto SiO_2/silicon substrates[68]. **k** | Typical angle-resolved photoemission spectroscopy image of the as-grown monolayer graphene on Cu(111)[91]. **l** | Scanning tunnelling spectroscopy spectra of the graphene films on Cu(111)[91]. E, E_F and K_y represent the kinetic energy of photoelectrons received by the analyser, the Fermi level energy and the momentum components along the K–M directions in the Brillouin zone, respectively. I and V represent the tunnelling current and the bias voltage, respectively. Parts **a, j** reprinted from REF.[68], Springer Nature Limited. Part **b** reprinted from REF.[69], Springer Nature Limited. Parts **c, i** adapted with permission from REF.[79], American Chemical Society. Parts **d, k, l** adapted from REF.[91], Springer Nature Limited. Parts **e, f** reprinted from REF.[81], Springer Nature Limited. Part **g** reprinted with permission from REF.[90], AAAS. Part **h** reprinted from REF.[95], Springer Nature Limited.

graphene, synthesizing TMDs requires more complicated growth parameters because of the solid precursors and phase control needed[10]. Compared with traditional solution-based polymerization, the CVD synthesis of polymeric thin films shows its unique advantages in terms of conformity and high purity[112].

CVD for 2D materials growth

CVD is the most widely used method for making high-quality monolayer TMDs in a laboratory setting[113–115]. The simplest method is thermal CVD[116], where powders of precursors are sublimated at high temperature to form a vapour that condenses as single-crystal monolayered TMDs on substrates without substrate-assisted catalysis. Thermal CVD results in deposition of discontinuous triangular crystals along with amorphous and multilayered products. Despite this, its simplicity and accessibility have made CVD the most widely studied and utilized method for synthesis of high-quality TMDs such as MoS_2, WS_2, WSe_2, $MoSe_2$ and their heterojunctions[117–119]. In thermal CVD synthesis of TMDs, the reaction chamber (usually a tube furnace, as shown in FIG. 5) is typically heated to 650–900 °C in a nitrogen (N_2) environment. At this high temperature, the precursor powder (such as MoO_3 for MoS_2) is reduced by the sulfur vapour to form volatile suboxides (for example, MoO_{3-x}).

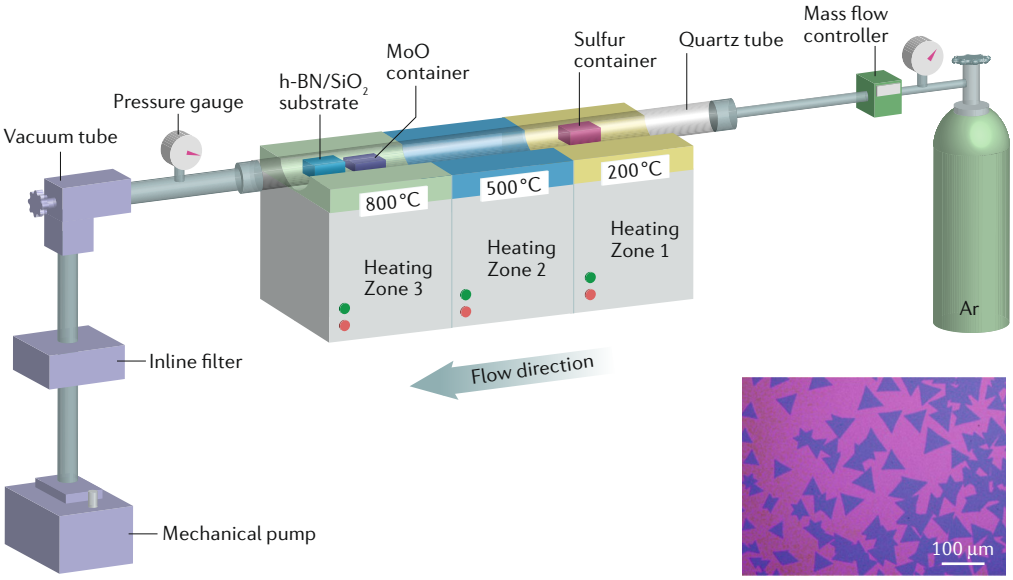

Fig. 5 | **Schematic of the typical components of a tube furnace used to grow MoS_2 and similar TMDs.** Typical reaction pathway for MoS_2 by thermal chemical vapour deposition (CVD): $MoO_3(s) + x/2S(g) \xrightarrow{650\ °C} MoO_{3-x}(g) + x/2SO_2$; bulk transport of MoO_{3-x} (g) and sulfur (g); surface adsorption of MoO_{3-x} (g) and S (g); $MoO_{3-x} + (3-x/2)S \xrightarrow{800\ °C} MoOS_2 + (1-x/2)SO_2$; $MoOS_2 \xrightarrow{800\ °C} MoS_2(s) + 1/2O_2(g)$; and bulk transport of O_2 away from the chamber. An optical microscopy image of typical triangular single-crystal MoS_2 monolayers is also shown[205]. h-BN, hexagonal boron nitride; TMD, 2D transition metal dichalcogenide. Adapted with permission from REF.[131], American Chemical Society. The optical microscopy image is adapted from REF.[205], Springer Nature Limited.

These suboxide compounds then diffuse to the substrate and further react with sulfur vapour to grow MoS_2 films in the form of triangles (shown in the optical microscopy image in FIG. 5) that are single layers.

Whereas uniform and continuous growth of TMDs with thermal CVD is difficult to achieve, some progress has been made in increasing the size of the monolayer crystals by adding salt (NaCl) to the precursors[120]. The role of salt is not yet clear but it likely facilitates the sublimation of transition metal precursors. However, the use of salt is problematic because sodium or chlorine can be introduced as impurities in the as-grown material. Theoretical work has shown that the presence of sodium on the substrate can influence the formation kinetics of MoS_2 (REF.[121]). The role of sodium on the rapid growth of MoS_2 was verified by producing large-area MoS_2 monolayers on soda-lime glass (composed of SiO_2, Na_2O and CaO)[122]. Another challenge in thermal CVD of TMDs is the nucleation of monolayers on technologically relevant substrates that are typically atomically smooth. Graphene-like molecules such as PTAS (perylene-3,4,9,10-tetracarboxylic acid tetrapotassium acid salt) and PTCDA (perylene-3,4,9,10-tetracarboxylic dianhydride) have been used as seed promoters and templated growth of TMDs[123]. In addition, as nucleation of monolayer crystals occurs at atomic edges, substrates such as sapphire with abundant atomic steps have also proved useful in achieving large monolayer crystals[124].

Recently, significant effort has been devoted to achieving highly uniform wafer-scale TMD films using MOCVD[123,125]. MOCVD vaporizes metal–organic precursors of both the transition metal and the chalcogen at lower than growth temperatures to achieve uniform monolayer TMDs. For MOCVD growth of wafer-scale MoS_2 and WS_2 (REF.[125]), molybdenum hexacarbonyl ($Mo(CO)_6$), tungsten hexacarbonyl ($W(CO)_6$) and diethyl sulfide ($(C_2H_4)_2S$) were used as sources of molybdenum, tungsten and sulfur, respectively. The precursors are directly introduced into a growth furnace heated at 550 °C in a hydrogen and argon atmosphere. The key to uniform and continuous monolayers with MOCVD is that the number of nucleation sites is kept low and the lateral growth from those nuclei is allowed to proceed very slowly — it took more than 26 h to fully cover the surface of a 4-inch silicon wafer (~10 cm in diameter)[125]. MOCVD also allows precise control of the concentration and supply of the precursors.

Similar to thermal CVD, alkali metal salts also play a crucial but somewhat unclear role in the synthesis of large domains and the suppression of nucleation sites in MOCVD. NaCl can suppress nucleation and achieve monolayer growth of MoS_2 (REFS[126,127]). In NaCl-assisted growth, the salt is typically placed with the substrates in the furnace, which is not a scalable strategy. The average lateral size of MoS_2 in salt-assisted growth was found to be ~60 µm with an electron mobility of 100 $cm^2 V^{-1} s^{-1}$ at cryogenic temperatures, indicating the high crystalline quality of the salt-assisted as-grown MoS_2 (REFS[128]).

The most common TMDs synthesized by thermal CVD and MOCVD are MoS_2, WS_2, $MoSe_2$ and WSe_2 (TABLE 3). Although significant effort has also been devoted to growing monolayers of metallic TMDs (for example, NbS_2, TaS_2 and VS_2)[129,130], these are difficult to grow with CVD because the powder transition metal or metal oxide precursors require very high processing

temperatures and equivalent metal organic precursors have yet to be developed. Despite this difficulty, CVD has been used to synthesize forms of niobium disulfide ($Nb_{1.35}S_2$) that possess very high electrical conductivity[130]. Molten salts can also play a role in reducing the melting points of precursors to form oxychlorides, which in turn can help with increasing the rate of growth of metallic TMDs. In a method for synthesizing metallic TMDs (TiS_2, $PtSe_2$, $PtTe_2$, NbS_2, $NbSe_2$, $NbTe_2$, VS_2, VSe_2 and so on) using molten salts[129], metal oxide precursors such as Nb_2O_5 were mixed with NaCl powder and thermal CVD used to grow triangular monolayers.

In addition to 2D TMDs, other 2D binary compounds such as h-BN, Mo_2C and ternary Bi_2O_2Se can also be successfully grown using CVD (TABLE 3). H-BN is a 2D insulator with a band gap of 5.9 eV, and plays important roles in advanced electronic devices as a gate dielectric layer or a protecting encapsulator. CVD growth of h-BN looks very similar to graphene in many aspects (substrate, carrier gas, temperature), except for the solid precursor ammonia borane (NH_3–BH_3), which is the most frequently used[99,131,132]. 2D Mo_2C, a 2D transition metal carbide, belongs to a family of materials that show many intriguing properties such as excellent catalytic activity and superconductivity. Large areas of Mo_2C have been grown using methane as a precursor and molybdenum as a substrate, where a copper foil on molybdenum melts during heating and forms a molybdenum–copper alloy that serves as a diffusion layer for molybdenum atoms and guarantees the chemical reaction leading to the formation of α-Mo_2C crystals[127]. Similarly, TaC can also be grown using tantalum as a substrate[133]. 2D Bi_2O_2Se is a semiconductor with high carrier mobility, in which the interaction between the charge-carried layers is stronger than the van der Waals interactions[134]. Therefore, to achieve atomically thin Bi_2O_2Se films and avoid vertical growth, mica and $SrTiO_3$ have been used as substrates to exploit the stronger interaction[20,135].

CVD for growing polymeric thin films

Complementing well-established solution-based methods, CVD extends the realm of utility for polymer thin films[112,136]. CVD is compatible with insoluble macromolecules, including many fluoropolymers, electrically conductive polymers and crosslinked organic networks. Its low growth temperatures (typically around 25 °C) and solvent-free nature allow CVD polymers to form directly on fragile substrates including papers, textiles and plant leaves, without a costly or complex transfer step. CVD polymerization can even be accomplished directly onto low-volatility liquid surfaces[112,137]. CVD polymers can have high purity as the small-molecule reactants used are easily purified and there is no possibility of residual solvent in the films[136]. Low defect levels are essential for device applications as well as for surfaces interacting with living cells and tissues[138], as highlighted below.

CVD polymeric layers can conformally follow the geometrical features of the underlying surface, yielding the same film thickness in all locations[139]. Such conformal coverage is essential for coating 3D devices, modifying the internal surfaces of porous materials and membranes, and for maintaining open pores in breathable fabrics and wearable electronics. By contrast, solution coatings are typically non-conformal, as surface tension can blanket the top of a porous surface without coating the interior of the pores. When blanketing closes off pores, surface area is lost for interfacial processes such as catalysis and molecular separations. Shear thinning, capillary forces and meniscus formation present in liquid-based coating processes also cause variations in film thickness over the geometric features in the substrate. The absence of surface tension in CVD processes also avoids pinhole formation by de-wetting even in sub-10 nm thick polymer films[112]. Ultrasmooth CVD polymers (<1 nm root mean square roughness) also reduce pinhole formation produced by excursions in surface roughness that exceed the film thickness.

Table 3 | **Summary of typical CVD methods for growing 2D materials**

Material	Substrate	Precursor 1	Precursor 2	Key parameters	Remarks	Refs
h-BN	Copper, nickel, platinum, SiO_2, sapphire	NH_3–BH_3 (heating at 60–100 °C)	–	LPCVD with H_2/argon flow, at ~1,000 °C	Single-crystal substrate with steps can induce the mono-orientation of h-BN	99,131,132
MS_2 (M = molybdenum, tungsten, etc.)	SiO_2, mica	Sulfur powder (heating at 100–200 °C)	MO_3 (near the hot centre)	APCVD or LPCVD, with H_2/argon flow at 600–900 °C	NaCl or KCl can serve as promoters for improving the quality and growth rate of these 2D TMDs	18,129,131
		$(C_2H_5)_2S$ (0.4 sccm)	–	MOCVD, at ~1,000 Pa, 550 °C		125
MSe_2 (M = molybdenum, tungsten, etc.)	SiO_2, mica	Selenium powder (heating at 200–300 °C)	MO_3 (near the hot centre)	APCVD or LPCVD, with H_2/argon flow, at 750–850 °C		117,129,195
Mo_2C, TaC	Molybdenum, tantalum	CH_4, C_2H_2	–	APCVD, at ~1,100 °C	Molten copper plays an important role in the catalytic growth process	127,133,196
Bi_2O_2Se	Mica, $SrTiO_3$	Bi_2Se_3 (heating at 650–700 °C)	Bi_2O_3 (heating at 650–700 °C)	LPCVD, with argon/O_2 flow at 500–600 °C	Substrate with quadruple symmetry ($SrTiO_3$) is important for epitaxial growth of single-crystal Bi_2O_2Se	20,135

APCVD, atmospheric pressure CVD; CVD, chemical vapour deposition; h-BN, hexagonal boron nitride; LPCVD, low-pressure CVD; MOCVD, metal–organic CVD; TMD, transition metal dichalcogenide.

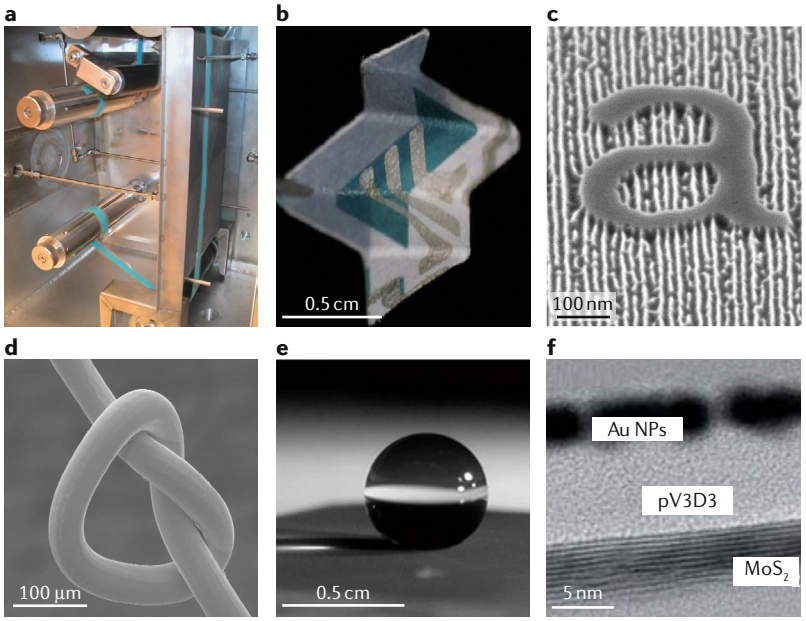

Fig. 6 | **Selected examples of CVD polymer processing and applications. a** | Roll-to-roll vacuum chamber, 300 mm wide, for chemical vapour deposition (CVD) polymerization[206]. **b** | A foldable solar cell, ~2 cm × 2 cm, fabricated directly on top of ordinary paper as the substrate, enabled by the low-temperature deposition and patterning of a CVD transparent conducting polymer[207]. **c** | Dual-scale pattern in silicon, including lines and spaces sub-10 nm, created using CVD polymerization[147]. **d** | Flexible and conformal CVD polymer encapsulation of a lead wire 25 µm in diameter for a biomedical implant[158]. **e** | A nearly spherical water drop on a superhydrophobic surface created by a CVD fluoropolymer grown conformally over a nanostructured array[208]. **f** | Ultrathin CVD polymer dielectric (pV3D3) for low-power flash memory[209]. NP, nanoparticle. Part **a** adapted with permission from REF.[206], The Royal Society of Chemistry. Part **b** adapted with permission from REF.[207], Wiley. Part **c** adapted from REF.[147], Springer Nature Limited. Part **d** adapted with permission from REF.[158], American Chemical Society. Part **e** adapted with permission from REF.[208], American Chemical Society. Part **f** adapted with permission from REF.[209], Wiley.

The properties and reactivity of CVD polymers can be tuned and optimized both at the surface and in the bulk via their organic functional groups[112,136]. To date, dozens of organic functional groups have been incorporated into CVD polymers and include amine, carboxylic acid, epoxy, hydroxyl, perfluorocarbon and zwitterionic moieties. Many of these organic functional groups permit further surface functionalization of CVD polymers with biomolecules and nanoparticles[136]. High densities of organic functional groups can lead to changes in film thickness and changes in properties in response to external variations such as temperature, humidity, light or pH[140,141]. Such responsive CVD polymers have been demonstrated for sensing and actuation, smart surfaces, molecular separations and controlled drug release[142–144].

The functional groups of CVD polymers can also be used to control surface energy from super-hydrophobic to super-hydrophilic. Low surface energy lubricious CVD polymer release layers are used commercially, for example in moulds used to manufacture rubber tyres and in seals and gaskets used in advanced manufacturing[145]. Hydrophobic CVD fluoropolymer conformal nanolayers maintain stamp feature fidelity during high-speed flexographic printing[146]. The precision of surface energy control achieved with conformal CVD polymers has also been exploited in directed self-assembly processes for defining features sub-10 nm and for patterning substrates with 3D topography[147–149].

Dielectric CVD polymers are commercially used for protection of electronic and medical devices[136]. CVD organic insulators have also been integrated into lightweight and mechanically flexible devices, including thin film transistors, logic circuits, flash memory and energy harvesting[112,150]. Conformal hybrid organic/inorganic polymer thin films containing boron or phosphorous have enabled the doping of 3D fin field-effect transistors[151].

Electrically conducting CVD polymers are attractive as flexible transparent conductors for optoelectronic devices, electrochemical energy storage and electrocatalysis[152]. The conductivity of CVD-grown polymer films can be 6,000 S cm^{-1} (REF.[153]), exceeding the values of all previously reported conducting polymer thin films[154] and reaching into the standard range for conductivity of brittle transparent inorganic conductors such as indium tin oxide (ITO). In addition, a resurgence of interest in the thermal properties of CVD conjugated polymers is driven by thermoelectric energy harvesting, as CVD polymers as thin as 2 nm have been incorporated into nanostructured energy storage devices[155] to increase pseudocapacitive charge storage. Selected examples of CVD polymer processing and applications are highlighted in FIG. 6.

Some, but not all, CVD polymerization methods use the same chemical reaction mechanisms (step growth, chain growth and condensation reactions) that underlie the synthesis of polymers in solution[136] (TABLE 4). Low surface growth temperatures (typically in the range of −10 to 140 °C) favour the adsorption of the CVD reactants, and traditional isotherms quantitatively describe monomer uptake on the growth surface[156]. Hence, knowledge of the saturation pressure of a new vapour phase reactant at the growth temperature allows the required CVD process conditions to be rapidly identified. This has been used for CVD growth of hundreds of different homopolymers, copolymers, crosslinked organic networks and organic/inorganic films[112], with well-defined growth kinetics providing reproducible growth even at sub-10 nm thickness[147]. Alternatively, the CVD conditions can be adjusted for rapid growth to produce films >10 µm thick[157].

Multiple strategies allow chemical covalent bonds to form between the substrate and the growing CVD polymer layer[112]. The resulting grafted interfaces greatly enhance durability. Avoiding delamination allows grafted CVD polymer films to be patterned and even to survive sandblasting. Durability is also enhanced by using crosslinked monomers, as crosslinked CVD organic networks display remarkable stability during multiple years of evaluation under physiological conditions[158].

Fundamental understanding of CVD polymerization aids the scale-up to cost-effective reactors >1 m in width and to economical roll-to-roll (R2R) processing[112], which is specifically detailed below (see Scaling up to factory-level application). Properties can be tuned and optimized through the selection of the volatile reactants and systematic variation of the CVD parameters such as flow rates, pressure and growth temperatures. Preserving

Delamination
A phenomenon in which layered composites, thin films or coatings separate from the adjacent layers or the substrate due to the weakening of the bonds holding the layers together.

Half-integer quantum Hall effect
A novel Hall effect quantized into a half-integer, owing to the peculiar nature of the Landau levels spectrum with energy spacing in graphene, where the Hall conductivity can be described as $\sigma_{xy} = 4e^2/h\left(N+\frac{1}{2}\right)$ (where h is Planck constant and $N = 0, 1, 2, \ldots$).

the fidelity of the monomeric structure in the polymer film is often key to optimizing properties. For example, preserving the structure of the monomer 3,4-ethylene dioxythiophene (EDOT) by oxidative CVD can produce electrical conductivity >6,000 S cm^{-1} (REF.[153]). By contrast, plasma-enhanced CVD does not fully retain the chemical structure of EDOT and the resulting films typically have poor electrical conductivity of <1 S cm^{-1} (REF.[152]).

Scaling up to factory-level application

The rapid progress in CVD graphene synthesis technology means it is the first reported 2D material to be scaled up at a factory level. Although we have known for more than 50 years that thin graphitic layers can be formed by CVD on nickel at high temperature using hydrocarbon sources such as methane[159,160], these graphitic layers were not monolayers owing to the high carbon solubility of nickel during the CVD process. This problem was solved by thermally depositing thin layers of nickel on SiO_2 substrates to limit the carbon concentration, leading to the formation of a centimetre-scale atomically thin layer of graphene[39,67]. CVD graphene was used to measure the half-integer quantum Hall effect originating from the ultra-high mobility of charge carriers in graphene for the first time[67,80], implying that the electrical performance of CVD graphene can be as good as mechanically exfoliated graphene. However, the non-uniform segregation of carbon sources from nickel limits the crystallinity of CVD graphene; this was overcome by using copper substrates that exhibit nearly zero carbon solubility, where the graphene layer is formed by the copper-mediated gradual surface diffusion and crystallization of adsorbed carbon atoms[38,160]. This self-limiting mechanism of graphene growth immediately enabled the wafer-scale synthesis of monolayer graphene[161], followed by the metre-scale growth of monolayer graphene by employing continuous R2R methods[162]. The large-area graphene synthesized by R2R technology has been utilized for practical applications such as flexible touch screens for mobile phones, flexible organic light-emitting diodes, flexible transparent heaters, electromagnetic wave interference shielding films and so on[36,163–165], which are expected to be commercialized in the near future.

R2R synthesis and its continuous processes are essential for the industrial commercialization of CVD graphene because it enables a >30-fold increase in productivity. These graphene synthesis capabilities with respect to the advances in CVD technology are highlighted in FIG. 7a. Although plasma-assisted low-temperature growth is helpful to simplify the equipment set-up and to save electrical energy, it always results in poor graphene electrical conductivity because of high defect density compared with graphene synthesized above 1,000 °C. In addition, putting multiple copper sheets in a CVD chamber can increase the synthesis capacity, but this type of batch synthesis remains limited by long heating and cooling times. In the R2R system, time is not wasted heating and cooling the CVD furnace; instead, the temperature in the furnace is kept constant while the copper foils pass through the hot zone at a rate of ~50 cm min^{-1}. R2R synthesis was first proposed in 2010 (REF.[162]), and additional R2R systems employing slightly different heater technologies were also developed[24,35,166,167]. For example, a microwave plasma technique was used to lower the synthesis temperature of the R2R process[35]; graphene films 230 mm wide and 120 m long were synthesized by applying high current through copper foils between the rolls[166]; an open chamber system was used to enable the R2R synthesis of graphene[168]; a concentric CVD reactor was used for high-speed R2R manufacturing of graphene films[169]; and the 190 mm-wide vertical R2R system with rapid thermal heaters enabled faster and more homogeneous heating[170]. More recently, the development of 500 mm-wide R2R systems capable of synthesizing graphene on copper foils ~100 m long at the rate of ~500 mm min^{-1} was reported[171].

The R2R method allows for the application of vertical tension to single-crystallize the copper foils and achieve higher quality graphene films. It is also applicable to post-CVD processes including etching and lamination (FIG. 7b), which are limited with batch-type CVD synthesis. R2R CVD synthesis is therefore considered the best way to mass-produce the CVD graphene films for commercial applications.

Although the scale-up for 2D materials synthesis is more complicated because it requires multiple precursors in different phases, various CVD methods used for graphene synthesis have been applied to the synthesis of other 2D materials. In general, powder sources are not favourable for factory-level synthesis of 2D materials because of the severe contamination of reaction chambers by residual solids. Compared with conventional CVD methods using liquid or solid precursors[123,125],

Table 4 | **Summary of CVD polymer growth methods**[a]

CVD polymerization method	Typical reactants	Analogous solution mechanism	Structure of polymer backbone	Refs
Initiated CVD	Initiator + monomer(s)	Chain growth	Carbon single bonds	142,197
Molecular layer deposition	Pair of monomers	Condensation	Includes heteroatoms (oxygen, nitrogen)	198,199
Oxidative CVD	Oxidant + monomer(s)	Step growth	Alternating single and double bonds	152,200,201
Poly(*p*-xylylenes) (parylene)	Dimer	None	Hydrocarbon	202,203
Plasma-enhanced CVD	Volatile precursor(s)	None	Various, typically crosslinked	204

CVD, chemical vapour deposition. [a]Typical reactants, solution-phase analogy and polymer backbone structure for different CVD polymerization methods.

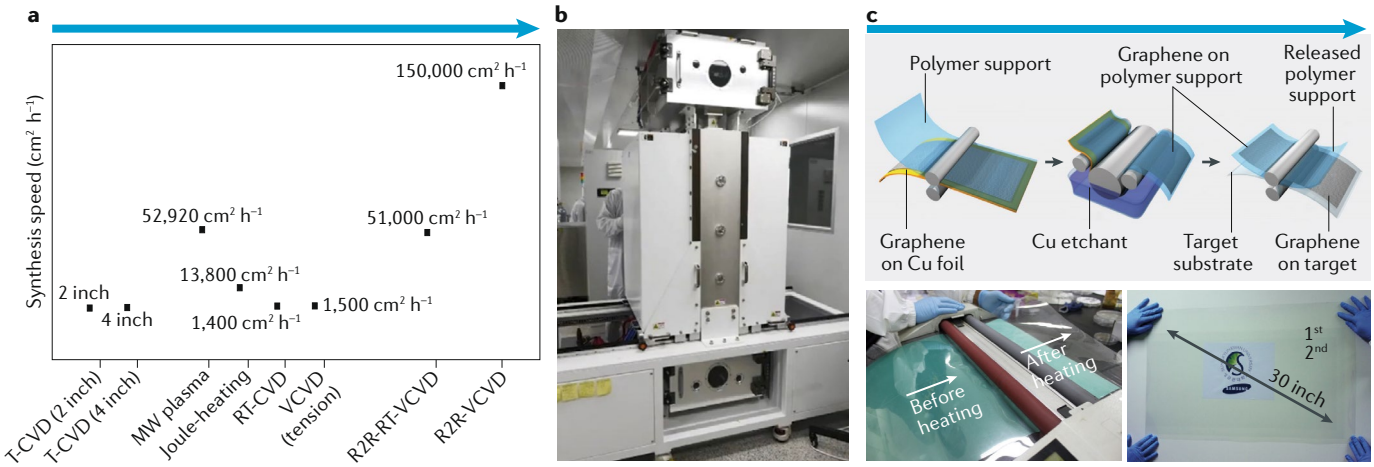

Fig. 7 | **Advances in CVD technology for scaling-up graphene synthesis. a** | Timeline highlighting the advances in chemical vapour deposition (CVD) technology to scale-up graphene synthesis from a manual 2-inch (5-cm) thermal CVD (T-CVD) furnace to a fully automated roll-to-roll (R2R) system 50 cm wide. **b** | A photo image of the 500 mm-wide vertical CVD (VCVD) system. **c** | Post-CVD processes that utilize the R2R method for the continuous production of graphene films, including etching and laminated transfer of CVD graphene films to target substrates[80]. MW, microwave; RT-CVD, rapid thermal CVD. Part **b** image courtesy of Yong Seok Choi, Graphene Square Inc. Part **c** adapted from REF.[80], Springer Nature Limited.

MOCVD is anticipated to be the best route to synthesize high-performance 2D materials larger than wafer scale[172]. The R2R CVD method has demonstrated the synthesis of MoS_2 films[173] as well as the synthesis of h-BN film on metal foils[174]. Atomic layer deposition also appears advantageous for the wafer-scale synthesis of high-mobility MoS_2 for practical applications[175].

As the CVD process is only one aspect of the full fabrication process to prepare graphene on target substrates, the post-CVD processes including etching and transfer need to be equally considered for factory-level scale-up. For example, the continuous synthesis of graphene by R2R methods must be followed by the R2R lamination of polymer supports[162], R2R removal of copper foils by chemical etchant or electrochemical etching[174] and patterning/transfer to target substrates[176]. The full R2R synthesis system is illustrated in FIG. 8.

Reproducibility and data deposition

The reproducibility and reliability of the performance of materials synthesized by CVD depend on both the pretreatment and post-CVD processes.

With respect to the pretreatment of substrates, we shall take as an example copper foils produced for general purposes. They are usually coated with an anti-oxidizing layer such as a type of chrome oxide, which needs to be removed by acid or thermal treatment[36] before graphene synthesis. In addition, these copper foils have usually been prepared by roll-pressing and are polycrystalline; they must be recrystallized to obtain larger single-crystalline graphene domains during deposition, as this is one of the crucial parameters minimizing defects and maximizing electrical conductivity. One approach is to mechanically strain the copper foil during CVD to transform polycrystalline copper to copper with very large single-crystal domains[177]. As the graphene and copper surfaces affect each other during growth, this causes the graphene-covered region in copper to undergo a drastic change in crystallinity[177]. An alternative approach is to prepare single-crystalline metal substrates by thermal annealing[178], an example of which is an annealed monocrystalline Cu(110) substrate used to synthesize highly crystalline large-area h-BN[132]. Another example is molten gold, which at high temperature catalyses the CVD growth of single-crystalline h-BN, where the small h-BN domains floating on the gold surface are rotated by electrostatic interaction to collimate each other to form a wafer-scale single crystalline film[179].

The uniformity of 2D materials synthesized by CVD generally depends on the uniformity of temperature and gas flow inside the reaction chamber[36]. For example, in the case of graphene synthesized by rapid thermal CVD, the temperature uniformity can be enhanced by using multi-zone rapid thermal heaters, where more than eight zones are separately controlled to balance the temperature distribution (FIG. 9a). The use of graphite susceptors that convert optical radiation to thermal energy is also useful to narrow down the temperature distribution. Most importantly, automated control to exclude human error is the key to reproducibility (see the less than 10% deviation of the graphene films sheet resistances from 10 different batches shown in FIG. 9b and their uniformity shown in FIG. 9c, satisfying industrial requirements). The durability of the electrical properties tested for the industrial standard (85% humidity at 85 °C) was measured to be suitable for practical applications (FIG. 9d).

As mentioned above, the CVD synthesis step is just one aspect of the full fabrication process, so the post-CVD processes including etching and transfer are as important as the CVD process to ensure reliability. In particular, the doping of graphene can increase the charge carrier density and considerably lower sheet resistance, which is desirable for practical applications[180]. In practice, the inhomogeneity and volatility of doping causes a reproducibility problem. The elemental doping of graphene that replaces carbon atoms with boron or nitrogen atoms is very stable and homogeneous, but it lowers charge carrier mobility due to electron scattering

around the heteroatoms[181] and decreases electrical conductivity, which is undesirable. In addition, although the non-destructive doping of graphene can be efficiently carried out by molecular dopants and self-assembled monolayers[182–184], it does not last long without proper encapsulation[185–187].

In summary, the reproducibility and reliability of the CVD-synthesized 2D materials largely depend on the surface freshness and the crystallinity of the catalytic substrates as well as the spatial uniformity of gas concentration and temperature, which need to be considered in designing CVD reactors.

Limitations and optimizations

The limitation of CVD technology often comes from the need for high temperature and high vacuum, particularly for graphene and h-BN synthesis. The most common chamber materials are quartz tubes that are thermally and mechanically strong enough to resist the reaction conditions. As the quartz reactors are scalable only up to 12-inch (~30 cm) diameters, stainless-steel chambers are alternatively used to design industrial-scale CVD reactors, where advanced chiller systems are essential to cool down the hot chamber and its housing. A quartz reactor is advantageous because it is standardized and replaceable at relatively low cost whenever the reactor is heavily contaminated. By contrast, a stainless steel reactor needs to be cleaned periodically to keep the quality of synthesis. The growth of other 2D materials at mild temperatures does not require quartz materials, but serious contamination of reaction chambers is often caused by residual precursors. Thus, the use of replaceable quartz tubes and gaseous precursors is recommended for 2D materials synthesis for industrial applications. In addition, a plasma module can be combined with thermal CVD systems to lower the synthesis temperature[188], but the high plasma energy often causes undesirable defects in the case of graphene.

The weight of copper foils needs to be considered in the design of the R2R synthesis system. The copper foil at ~1,000 °C becomes less stiff and more ductile, so the horizontal tension across the rolls 2–3 m long results in serious deformation. This can be minimized by vertical loading parallel to the gravitational force and winding tension[177]. In addition, the vertical tension control is useful to promote the growth of single-crystalline copper foils for high-quality graphene synthesis[177].

To facilitate the optimization processes of CVD synthesis, high-throughput in situ quality assessment tools for graphene and 2D materials are of great importance. As CVD often involves high temperatures and vacuum conditions, in situ monitoring is possible only by an optical method equipped with fibre and lens optics that can collect signals through the optical window of CVD chambers. For this reason, Raman spectroscopy has been investigated as a characterization tool to examine the number of layers, defect density and coverage of graphene and 2D materials[101]. However, its field of view and scanning speed are not large and fast enough for factory-level real-time assessment, respectively. Wide-field Raman spectroscopy that scans only D and G peak ranges is much faster, but requires extremely powerful laser sources incompatible with commercial instrumentation[189]. Microwave spectroscopy using an eddy current[190] and terahertz time-domain spectroscopy[191] have enabled the fast analysis of wafer-scale graphene, but these methods are valid only for post-CVD graphene transferred to insulating substrates. In terms of industrial quality control, the evaluation of graphene as grown on copper foil is more important to optimize the growth conditions. Confocal laser scanning microscopy (CLSM) is expected to satisfy the above-mentioned demands for real-time assessment regardless of production scale[192]. The CLSM image contrast between graphene and copper substrate is found to be inversely proportional to the defect density, and therefore the electrical conductivity can be briefly monitored by fast scanning by CLSM[170] (FIG. 10). It can be also applied to the quality assessment of other 2D materials, although the laser wavelengths of CLSM need to be optimized on a case by case basis.

Outlook

CVD reactors require relatively inexpensive components and are simple to set up, which has led to their widespread use in the academic community for easily producing novel materials such as graphene, 2D semiconductors and polymer thin films. However, CVD itself is a mature commercial technology for applying thin films on various components and is particularly useful in the electronics industry, where large-area and continuous deposition of thin films can be performed in specially designed reactors. Examples of these include vertical reactors for floating catalytic synthesis of carbon nanotubes[193,194] or R2R CVD systems for graphene

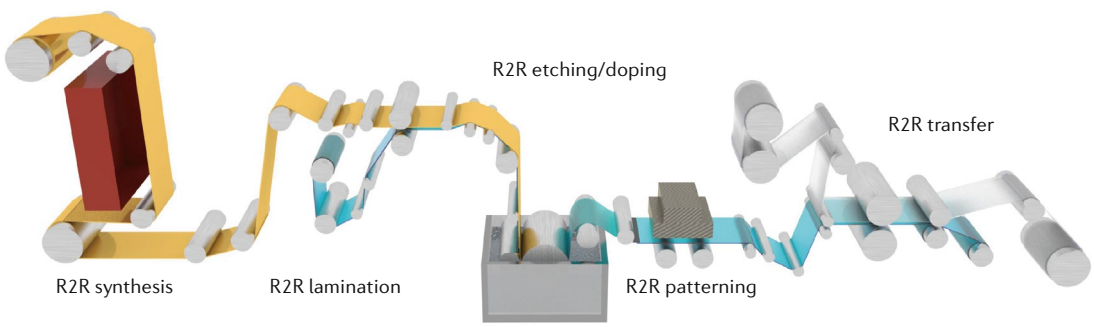

Fig. 8 | **Full R2R production of graphene films.** Roll-to-roll (R2R) chemical vapour deposition (CVD) synthesis of graphene on copper (yellow), R2R lamination, R2R etching/doping and R2R patterning/transfer to target substrates (blue) for graphene film production. Figure reprinted from REF.[170], CC BY 4.0 (https://www.creativecommons.org/licenses/by/4.0/).

growth[177]. The fundamental limitation of CVD is that it often requires a high temperature (typically >400 °C) to crack the precursors into reactive products that can readily form thin films (especially for graphene and h-BN). Lower deposition temperatures can be achieved by utilizing plasma to produce excited state or ionized precursors that can react at low temperatures. The ability to deposit high-quality films at low temperatures (typically <400 °C) is highly desirable in back end of line processes for electronics, thermosensitive substrates and soft metals. The critical challenges that remain in low-temperature CVD for growing inorganic materials are lack of crystallinity, trapped precursors and maintenance of the desired stoichiometry.

CVD is the most widely used method for large-area synthesis of advanced low-dimensional materials such as nanowires, nanotubes and, more recently, 2D materials, and is exclusively used for large-area synthesis of graphene. Whereas very high-quality graphene films can now be achieved over metre scales using CVD, a remaining challenge is that the growth is limited to copper (or its alloy). This is a challenge because in order to use graphene for electronics, optics and other applications, it must be transferred onto a desired substrate. A substantial amount of research has been devoted to clean transfer of graphene from copper onto arbitrary substrates. This research has led to substantial progress and demonstrations that high-quality graphene can be transferred onto virtually any substrate. However, the risk of tears and wrinkles along with incorporation of copper or transfer solvent impurities remain. Thus, research in contamination and damage-free transfer must continue. The ultimate achievement for CVD of graphene would be the development of a process that allows direct growth of graphene on any substrate. In particular, the direct, large-area and local growth of graphene on insulating wafers used in electronics would be a major breakthrough.

The research in 2D semiconductors — in particular, TMDs — has clearly shown that they hold tremendous promise for electronics and other applications. A major bottleneck for their implementation is the absence of a CVD process that allows the realization of high-quality

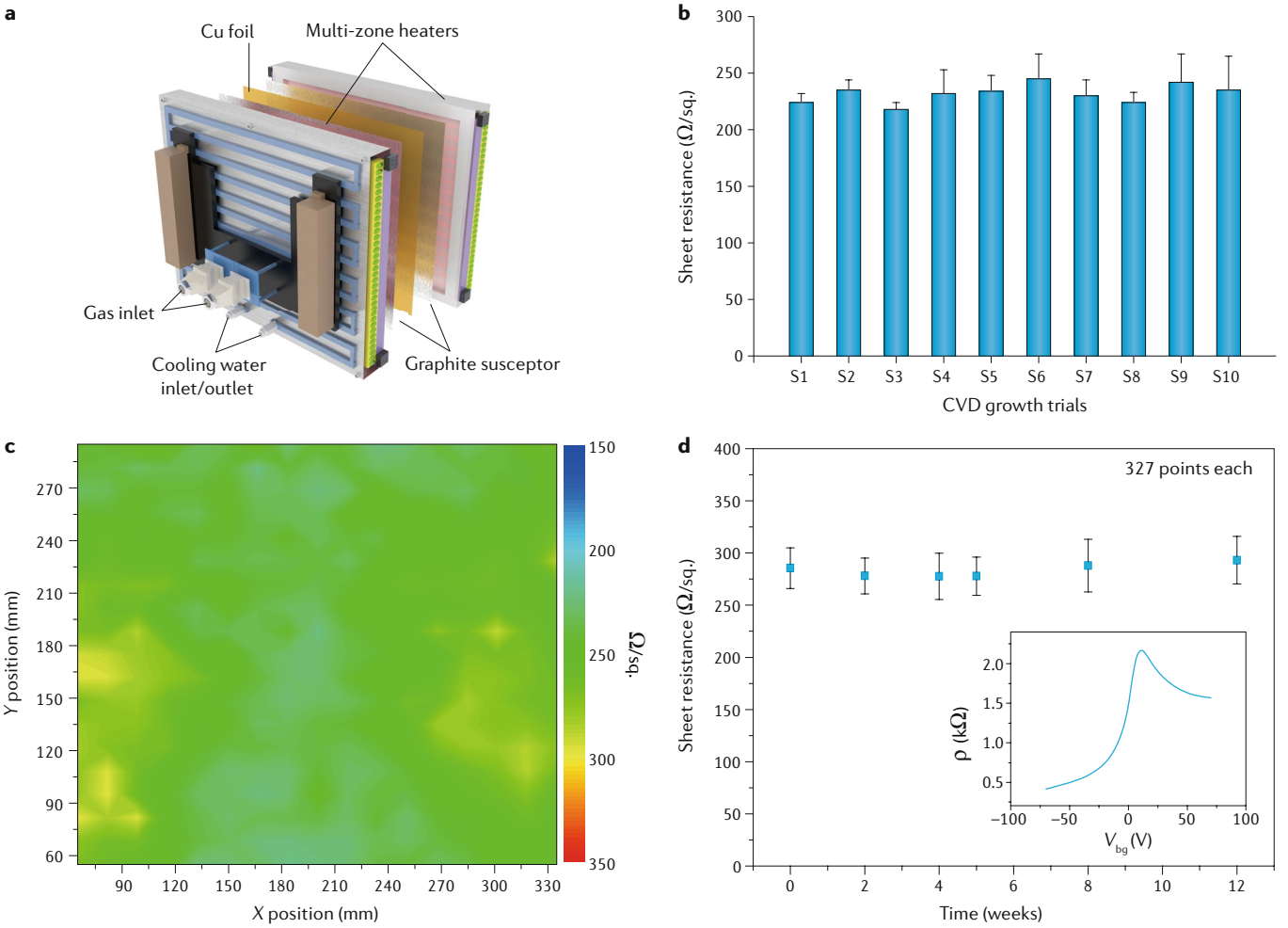

Fig. 9 | **Important factors that determine the reliability of graphene synthesis, and the corresponding electrical performance data. a** | Multi-zone heaters with graphite susceptors. **b** | Reproducibility of sheet resistance for 10 different growth trials. **c** | Spatial sheet resistance distribution of the graphene films. **d** | Time-durability of the graphene films monitored at 85 °C with 85% humidity for 12 weeks. Inset: resistivity (ρ) of the graphene synthesized by rapid thermal chemical vapour deposition (CVD) as a function of back gate voltage (V_{bg}) at room temperature, which indicates the carrier mobility is as high as 5290 $cm^2 V^{-1} s^{-1}$. Parts **a**–**d** adapted with permission from REF.[36], American Chemical Society.

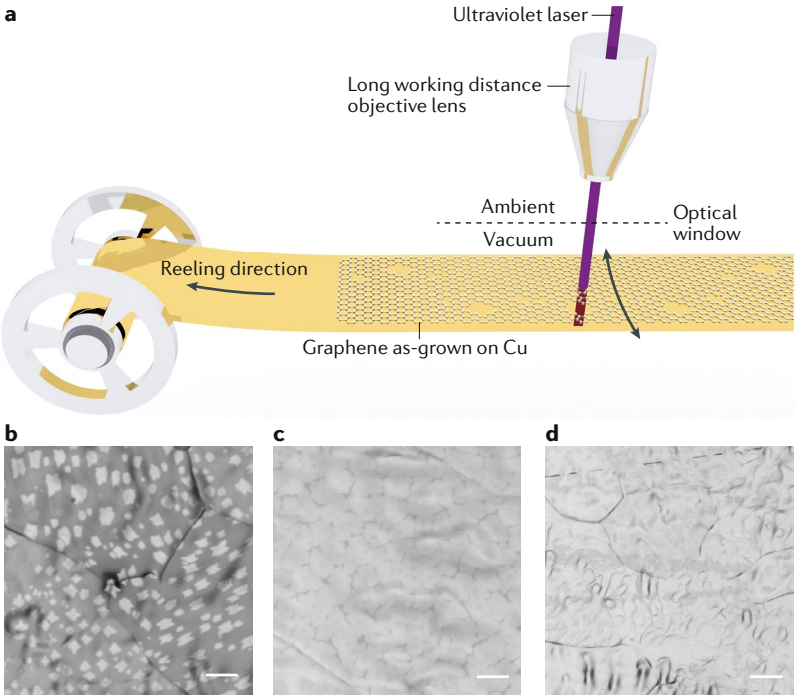

Fig. 10 | **Concept of in situ monitoring of the as-grown CVD graphene on copper using CLSM. a** | Concept of monitoring the as-grown chemical vapour deposition (CVD) graphene on copper foil during the continuous roll-to-roll synthetic process using reflective mode confocal laser scanning microscopy (CLSM). **b**–**d** | CLSM images of the CVD graphene grown for 10 min (part **b**), 13 min (part **c**) and 30 min (part **d**). Scale bar: 10 µm. Parts **a**–**d** reprinted from REF.[170], CC BY 4.0 (https://www.creativecommons.org/licenses/by/4.0/).

large-area (for example, wafer scale) thin films. The advantage of TMD films — in contrast to graphene growth — is that they can be directly grown on insulating substrates but centimetre-scale single-crystal (or even large grained) thin films are still challenging. MOCVD has shown promise in achieving uniform wafer-scale atomically thin films of semiconducting 2D materials such as MoS_2 and WS_2 with nanoscale domain sizes, but additional work is needed to increase the size of the crystals in the atomically thin films and minimize the concentration of grain boundaries. Uniform growth of single-crystal 2D thin films therefore requires knowledge of the nucleation and growth mechanisms that must be established through detailed analyses of the reactive gas phase, surface phenomena and measurements during MOCVD growth. In addition to semiconducting 2D materials, metallic compounds (such as NbS_2 and VS_2) are interesting from both fundamental and technological viewpoints, because high-quality metallic 2D compounds synthesized via MOCVD could hold promise for high-performance contacts and interconnects. Another interesting direction of research in 2D semiconductors is the integration of different materials by stacking. To exploit the optoelectronic properties of vertically stacked heterostructures, different TMD layers must be grown on each other. Some preliminary results suggest that this is possible but more work is needed to realize wafer-scale stacked 2D layers.

A fundamental problem that is rarely discussed in CVD of 2D semiconductors — in particular, TMDs — is that high-temperature deposition and subsequent cooling leads to by-products of chalcogen (sulfur, selenium, tellurium) species (for example, sub-stoichiometric compounds). Decreasing the temperature compromises the crystalline quality of the TMD films. Thus, development of deposition and cooling processes are required to ensure that the deposited atomically thin films are indeed stoichiometric. Finally, the dearth of MOCVD precursors means that only a handful of 2D semiconductor compounds can be grown. This means that many interesting TMD compounds — in particular, metallic ones — cannot currently be deposited by MOCVD. Efforts to expand the number and type of precursors will benefit the growth community in realizing new compounds as well as perfecting the growth of existing capabilities. A challenge with MOCVD is that the precursors are toxic, and thus specialized spaces with appropriate safety precautions are needed to carry out the experiments. Development of benign precursors could also lead to more widespread adoption of MOCVD and accelerate the development of 2D thin films.

To summarize, the key challenges to be addressed in CVD of 2D materials are: lowering the deposition temperature; uniform and large-area growth on various substrates; and developing benign precursors for MOCVD growth of a wide range of TMD materials.

In this Primer, we have presented a comprehensive overview of CVD methods. We have included the instrument construction and the process of material preparation and characterization, concentrating on the growth of graphene and other 2D materials such as TMDs and polymeric thin films. The recent advances and challenges of this technique in terms of mass production, controllability, reproducibility, cost and online monitoring have also been highlighted, in the hope of underscoring the importance of CVD and the benefit it can bring to modern industry.

Published online: 14 January 2021

1. Teal, G. K., Fisher, J. R. & Treptow, A. W. A new bridge photo-cell employing a photo-conductive effect in silicon. Some properties of high purity silicon. *J. Appl. Phys.* **17**, 879–886 (1946).
2. Carlson, D. E. & Wronski, C. R. Amorphous silicon solar cell. *Appl. Phys. Lett.* **28**, 671–673 (1976).
3. Knights, J. C. Substitutional doping in amorphous silicon. *Am. Inst. Phys. Conf. Ser.* **31**, 296–300 (1976).
4. Manasevit, H. M. Recollections and reflections of MO-CVD. *J. Cryst. Growth* **55**, 1–9 (1981).
5. Tsang, W. T. Chemical beam epitaxy of InP and GaAs. *Appl. Phys. Lett.* **45**, 1234–1236 (1984).
6. Xia, Y. et al. One-dimensional nanostructures: synthesis, characterization, and applications. *Adv. Mater.* **15**, 353–389 (2003).
7. Novoselov, K. S. et al. Electric field effect in atomically thin carbon films. *Science* **306**, 666–669 (2004).
8. Novoselov, K. S. et al. A roadmap for graphene. *Nature* **490**, 192–200 (2012).
9. Lin, L., Deng, B., Sun, J., Peng, H. & Liu, Z. Bridging the gap between reality and ideal in chemical vapor deposition growth of graphene. *Chem. Rev.* **118**, 9281–9343 (2018).
This review provides a systematic introduction to the CVD growth of graphene.
10. Cai, Z., Liu, B., Zou, X. & Cheng, H. M. Chemical vapor deposition growth and applications of two-dimensional materials and their heterostructures. *Chem. Rev.* **118**, 6091–6133 (2018).
This paper is a systematic introduction to CVD growth of 2D materials and their heterostructures.
11. Choy, K. L. Chemical vapour deposition of coatings. *Prog. Mater. Sci.* **48**, 57–170 (2003).
12. Yan, K., Fu, L., Peng, H. L. & Liu, Z. F. Designed CVD growth of graphene via process engineering. *Acc. Chem. Res.* **46**, 2263–2274 (2013).
13. Wang, H. et al. Primary nucleation-dominated chemical vapor deposition growth for uniform graphene monolayers on dielectric substrate. *J. Am. Chem. Soc.* **141**, 11004–11008 (2019).

14. Xie, H. et al. H_2O-etchant-promoted synthesis of high-quality graphene on glass and its application in see-through thermochromic displays. *Small* **16**, e1905485 (2020).
15. Park, J. H. et al. Large-area monolayer hexagonal boron nitride on Pt foil. *ACS Nano* **8**, 8520–8528 (2014).
16. Zhang, Z. W. et al. Robust epitaxial growth of two-dimensional heterostructures, multiheterostructures, and superlattices. *Science* **357**, 788–792 (2017).
17. Sahoo, P. K., Memaran, S., Xin, Y., Balicas, L. & Gutierrez, H. R. One-pot growth of two-dimensional lateral heterostructures via sequential edge-epitaxy. *Nature* **553**, 63–67 (2018).
18. Ji, Q. et al. Epitaxial monolayer MoS_2 on mica with novel photoluminescence. *Nano Lett.* **13**, 3870–3877 (2013).
19. Zhang, Y. et al. Controlled growth of high-quality monolayer WS_2 layers on sapphire and imaging its grain boundary. *ACS Nano* **7**, 8963–8971 (2013).
20. Wu, J. et al. Controlled synthesis of high-mobility atomically thin bismuth oxyselenide crystals. *Nano Lett.* **17**, 3021–3026 (2017).
21. Jia, K. C. et al. Copper-containing carbon feedstock for growing superclean graphene. *J. Am. Chem. Soc.* **141**, 7670–7674 (2019).
22. Wang, H. et al. Synthesis of boron-doped graphene monolayers using the sole solid feedstock by chemical vapor deposition. *Small* **9**, 1316–1320 (2013).
23. Jiang, B. et al. Batch synthesis of transfer-free graphene with wafer-scale uniformity. *Nano Res.* **13**, 1564–1570 (2020).
24. Deng, B. et al. Roll-to-roll encapsulation of metal nanowires between graphene and plastic substrate for high-performance flexible transparent electrodes. *Nano Lett.* **15**, 4206–4213 (2015).
25. Deng, B. et al. Scalable and ultrafast epitaxial growth of single-crystal graphene wafers for electrically tunable liquid-crystal microlens arrays. *Sci. Bull.* **64**, 659–668 (2019).
26. Tang, L. et al. Vertical chemical vapor deposition growth of highly uniform 2D transition metal dichalcogenides. *ACS Nano* **4**, 4646–4653 (2020).
27. Xu, J. et al. Fast batch production of high-quality graphene films in a sealed thermal molecular movement system. *Small* **13**, 1700651 (2017).
28. Li, Y. et al. Large single-crystal Cu foils with high-index facets by strain-engineered anomalous grain growth. *Adv. Mater* **32**, e2002034 (2020).
29. Deng, B., Liu, Z. & Peng, H. Toward mass production of CVD graphene films. *Adv. Mater* **31**, e1800996 (2018).
30. Chen, X. D. et al. Fast growth and broad applications of 25-inch uniform graphene glass. *Adv. Mater.* **29**, e1603428 (2017).
31. Sun, Z. Z. et al. Large-area bernal-stacked Bi-, Tr-, and tetralayer graphene. *ACS Nano* **6**, 9790–9796 (2012).
32. Xu, Y. & Yan, X.-T. *Chemical Vapour Deposition: An Integrated Engineering Design for Advanced Materials* (Springer, 2010).
33. Bointon, T. H., Barnes, M. D., Russo, S. & Craciun, M. F. High quality monolayer graphene synthesized by resistive heating cold wall chemical vapor deposition. *Adv. Mater.* **27**, 4200–4206 (2015).
34. Qi, Y. et al. Switching vertical to horizontal graphene growth using faraday cage-assisted PECVD approach for high-performance transparent heating device. *Adv. Mater.* **30**, e1704839 (2018).
35. Yamada, T., Ishihara, M., Kim, J., Hasegawa, M. & Iijima, S. A roll-to-roll microwave plasma chemical vapor deposition process for the production of 294 mm width graphene films at low temperature. *Carbon* **50**, 2615–2619 (2012).
36. Ryu, J. et al. Fast synthesis of high-performance graphene films by hydrogen-free rapid thermal chemical vapor deposition. *ACS Nano* **8**, 950–956 (2014).
37. Piner, R. et al. Graphene synthesis via magnetic inductive heating of copper substrates. *ACS Nano* **7**, 7495–7499 (2013).
38. Li, X. et al. Large-area synthesis of high-quality and uniform graphene films on copper foils. *Science* **324**, 1312 (2009).
This paper is the first report of large-area monolayer graphene films via CVD.
39. Reina, A. et al. Large area, few-layer graphene films on arbitrary substrates by chemical vapor deposition. *Nano Lett.* **9**, 30–35 (2009).
40. Chen, J. et al. Oxygen-aided synthesis of polycrystalline graphene on silicon dioxide substrates. *J. Am. Chem. Soc.* **133**, 17548–17551 (2011).
41. Chen, Z. et al. High-brightness blue light-emitting diodes enabled by a directly grown graphene buffer layer. *Adv. Mater.* **30**, e1801608 (2018).
42. Chen, Z., Qi, Y., Chen, X., Zhang, Y. & Liu, Z. Direct CVD growth of graphene on traditional glass: methods and mechanisms. *Adv. Mater.* **31**, e1803639 (2019).
43. Hao, Y. F. et al. The role of surface oxygen in the growth of large single-crystal graphene on copper. *Science* **342**, 720–723 (2013).
44. Sun, L. et al. Visualizing fast growth of large single-crystalline graphene by tunable isotopic carbon source. *Nano Res.* **10**, 355–363 (2016).
45. Xu, X. et al. Ultrafast epitaxial growth of metre-sized single-crystal graphene on industrial Cu foil. *Sci. Bull.* **62**, 1074–1080 (2017).
This report highlights the transformation of polycrystalline metal foil into a single-crystal one for high-quality graphene growth.
46. Wu, M. et al. Seeded growth of large single-crystal copper foils with high-index facets. *Nature* **581**, 406–410 (2020).
47. Li, Y., Sun, L., Liu, H., Wang, Y. & Liu, Z. Preparation of single-crystal metal substrates for the growth of high-quality two-dimensional materials. *Inorg. Chem. Front.* https://doi.org/10.1039/D1030QI00923G (2020).
48. German, E. D. & Sheintuch, M. Predicting CH_4 dissociation kinetics on metals: trends, sticking coefficients, H tunneling, and kinetic isotope effect. *J. Phys. Chem. C.* **117**, 22811–22826 (2013).
49. Li, X. S. et al. Graphene films with large domain size by a two-step chemical vapor deposition process. *Nano Lett.* **10**, 4328–4334 (2010).
50. Bhaviripudi, S., Jia, X., Dresselhaus, M. S. & Kong, J. Role of kinetic factors in chemical vapor deposition synthesis of uniform large area graphene using copper catalyst. *Nano Lett.* **10**, 4128–4133 (2010).
51. Lin, L. et al. Towards super-clean graphene. *Nat. Commun.* **10**, 1912 (2019).
52. Sun, J. et al. Direct chemical vapor deposition-derived graphene glasses targeting wide ranged applications. *Nano Lett.* **15**, 5846–5854 (2015).
53. Li, X. S., Cai, W. W., Colombo, L. & Ruoff, R. S. Evolution of graphene growth on Ni and Cu by carbon isotope labeling. *Nano Lett.* **9**, 4268–4272 (2009).
54. Dai, B. et al. Rational design of a binary metal alloy for chemical vapour deposition growth of uniform single-layer graphene. *Nat. Commun.* **2**, 522 (2011).
55. Liu, X. et al. Segregation growth of graphene on Cu–Ni alloy for precise layer control. *J. Phys. Chem. C.* **115**, 11976–11982 (2011).
56. Li, Y., Sun, L., Liu, H., Wang, Y. & Liu, Z. Rational design of binary alloys for catalytic growth of graphene via chemical vapor deposition. *Catalysts* **10**, 1305 (2020).
57. Liu, N. et al. The origin of wrinkles on transferred graphene. *Nano Res.* **4**, 996–1004 (2011).
58. Deng, B. et al. Wrinkle-free single-crystal graphene wafer grown on strain-engineered substrates. *ACS Nano* **11**, 12337–12345 (2017).
59. Zhang, C., Fu, L., Zhang, Y. & Liu, Z. Segregation phenomenon and its control in the catalytic growth of graphene. *Acta Chim. Sin.* **71**, 308–308 (2013).
60. Deng, B. et al. Anisotropic strain relaxation of graphene by corrugation on copper crystal surfaces. *Small* **14**, e1800725 (2018).
61. Yu, S. U. et al. Simultaneous visualization of graphene grain boundaries and wrinkles with structural information by gold deposition. *ACS Nano* **8**, 8662–8668 (2014).
62. Massalski, T. B., Murray, J. L., Bennet, L. H. & Baker, H. *Binary Alloy Phase Diagrams* (ASM International, 1986).
63. Dwight E. Gray, A. I. O. P. *American Institute of Physics Handbook* 3rd edn (McGraw-Hill, 1972).
64. Reina, A. et al. Growth of large-area single- and Bi-layer graphene by controlled carbon precipitation on polycrystalline Ni surfaces. *Nano Res.* **2**, 509–516 (2009).
65. Yan, K. et al. Modulation-doped growth of mosaic graphene with single-crystalline p–n junctions for efficient photocurrent generation. *Nat. Commun.* **3**, 1280 (2012).
66. Blake, P. et al. Making graphene visible. *Appl. Phys. Lett.* **91**, 063124 (2007).
67. Kim, K. S. et al. Large-scale pattern growth of graphene films for stretchable transparent electrodes. *Nature* **457**, 706–710 (2009).
68. Huang, M. et al. Large-area single-crystal AB-bilayer and ABA-trilayer graphene grown on a Cu/Ni(111) foil. *Nat. Nanotechnol.* **15**, 289–295 (2020).
69. Gao, L. B. et al. Repeated growth and bubbling transfer of graphene with millimetre-size single-crystal grains using platinum. *Nat. Commun.* **3**, 699 (2012).
70. Duong, D. L. et al. Probing graphene grain boundaries with optical microscopy. *Nature* **490**, 235–239 (2012).
71. Gan, L. & Luo, Z. T. Turning off hydrogen to realize seeded growth of subcentimeter single-crystal graphene grains on copper. *ACS Nano* **7**, 9480–9488 (2013).
72. Ly, T. H. et al. Nondestructive characterization of graphene defects. *Adv. Funct. Mater.* **23**, 5183–5189 (2013).
73. Kong, X. H. et al. Non-destructive and rapid evaluation of chemical vapor deposition graphene by dark field optical microscopy. *Appl. Phys. Lett.* **103**, 043119 (2013).
74. Huang, L. et al. Twinkling graphene on polycrystalline Cu substrate: a scanning electron microscopy study. *J. Appl. Phys.* **125**, 194303 (2019).
75. Huang, L. et al. High-contrast SEM imaging of supported few-layer graphene for differentiating distinct layers and resolving fine features: there is plenty of room at the bottom. *Small* **14**, e1704190 (2018).
76. Wang, Z. J. et al. Direct observation of graphene growth and associated copper substrate dynamics by in situ scanning electron microscopy. *ACS Nano* **9**, 1506–1519 (2015).
77. Lee, C., Wei, X. D., Kysar, J. W. & Hone, J. Measurement of the elastic properties and intrinsic strength of monolayer graphene. *Science* **321**, 385–388 (2008).
78. Sun, L. et al. A force-engineered lint roller for superclean graphene. *Adv. Mater.* **31**, 1902978 (2019).
79. Kang, J. H. et al. Strain relaxation of graphene layers by Cu surface roughening. *Nano Lett.* **16**, 5993–5998 (2016).
80. Bae, S. et al. Roll-to-roll production of 30-inch graphene films for transparent electrodes. *Nat. Nanotechnol.* **5**, 574–578 (2010).
This report highlights the large-scale growth and transfer of graphene films.
81. Yu, Q. K. et al. Control and characterization of individual grains and grain boundaries in graphene grown by chemical vapour deposition. *Nat. Mater.* **10**, 443–449 (2011).
82. Levy, N. et al. Strain-induced pseudo-magnetic fields greater than 300 tesla in graphene nanobubbles. *Science* **329**, 544–547 (2010).
83. Lahiri, J., Lin, Y., Bozkurt, P., Oleynik, I. I. & Batzill, M. An extended defect in graphene as a metallic wire. *Nat. Nanotechnol.* **5**, 326–329 (2010).
84. Artyukhov, V. I., Liu, Y. Y. & Yakobson, B. I. Equilibrium at the edge and atomistic mechanisms of graphene growth. *Proc. Natl Acad. Sci. USA* **109**, 15136–15140 (2012).
85. Shu, H. B., Chen, X. S., Tao, X. M. & Ding, F. Edge structural stability and kinetics of graphene chemical vapor deposition growth. *ACS Nano* **6**, 3243–3250 (2012).
86. Yuan, Q. H. et al. Magic carbon clusters in the chemical vapor deposition growth of graphene. *J. Am. Chem. Soc.* **134**, 2970–2975 (2012).
87. Rasool, H. I. et al. Continuity of graphene on polycrystalline copper. *Nano Lett.* **11**, 251–256 (2011).
88. Rasool, H. I. et al. Atomic-scale characterization of graphene grown on copper(100) single crystals. *J. Am. Chem. Soc.* **133**, 12536–12543 (2011).
89. Yang, W. et al. Epitaxial growth of single-domain graphene on hexagonal boron nitride. *Nat. Mater.* **12**, 792–797 (2013).
90. Liu, L. et al. Heteroepitaxial growth of two-dimensional hexagonal boron nitride templated by graphene edges. *Science* **343**, 163–167 (2014).
91. Yuan, G. W. et al. Proton-assisted growth of ultra-flat graphene films. *Nature* **577**, 204–208 (2020).
92. Sutter, E., Acharya, D. P., Sadowski, J. T. & Sutter, P. Scanning tunneling microscopy on epitaxial bilayer graphene on ruthenium(0001). *Appl. Phys. Lett.* **94**, 133101 (2009).
93. Gao, L., Guest, J. R. & Guisinger, N. P. Epitaxial graphene on Cu(111). *Nano Lett.* **10**, 3512–3516 (2010).
94. Hashimoto, A., Suenaga, K., Gloter, A., Urita, K. & Iijima, S. Direct evidence for atomic defects in graphene layers. *Nature* **430**, 870–873 (2004).
95. Huang, P. Y. et al. Grains and grain boundaries in single-layer graphene atomic patchwork quilts. *Nature* **469**, 389–392 (2011).

96. Kim, K. et al. Grain boundary mapping in polycrystalline graphene. *ACS Nano* **5**, 2142–2146 (2011).
97. Lee, J. H. et al. Wafer-scale growth of single-crystal monolayer graphene on reusable hydrogen-terminated germanium. *Science* **344**, 286–289 (2014).
98. Jiang, Y. et al. Electron ptychography of 2D materials to deep sub-angstrom resolution. *Nature* **559**, 343–349 (2018).
99. Chen, T. A. et al. Wafer-scale single-crystal hexagonal boron nitride monolayers on Cu(111). *Nature* **579**, 219–223 (2020).
100. Xu, X. Z. et al. Ultrafast growth of single-crystal graphene assisted by a continuous oxygen supply. *Nat. Nanotechnol.* **11**, 930–935 (2016).
101. Ferrari, A. C. & Basko, D. M. Raman spectroscopy as a versatile tool for studying the properties of graphene. *Nat. Nanotechnol.* **8**, 235–246 (2013).
This paper highlights the utility of Raman spectroscopy for characterizing the properties of graphene.
102. Ferrari, A. C. et al. Raman spectrum of graphene and graphene layers. *Phys. Rev. Lett.* **97**, 187401 (2006).
103. Das, A. et al. Monitoring dopants by Raman scattering in an electrochemically top-gated graphene transistor. *Nat. Nanotechnol.* **3**, 210–215 (2008).
104. Lee, J. E., Ahn, G., Shim, J., Lee, Y. S. & Ryu, S. Optical separation of mechanical strain from charge doping in graphene. *Nat. Commun.* **3**, 1024 (2012).
105. Bronsgeest, M. S. et al. Strain relaxation in CVD graphene: wrinkling with shear lag. *Nano Lett.* **15**, 5098–5104 (2015).
106. Zhao, T. et al. Ultrafast growth of nanocrystalline graphene films by quenching and grain-size-dependent strength and bandgap opening. *Nat. Commun.* **10**, 4854 (2019).
107. Varykhalov, A. et al. Electronic and magnetic properties of quasifreestanding graphene on Ni. *Phys. Rev. Lett.* **101**, 157601 (2008).
108. Avila, J. et al. Exploring electronic structure of one-atom thick polycrystalline graphene films: a nano angle resolved photoemission study. *Sci. Rep.* **3**, 2439 (2013).
109. Varykhalov, A., Scholz, M. R., Kim, T. K. & Rader, O. Effect of noble-metal contacts on doping and band gap of graphene. *Phys. Rev. B* **82**, 121101 (2010).
110. Gottardi, S. et al. Comparing graphene growth on Cu(111) versus oxidized Cu(111). *Nano Lett.* **15**, 917–922 (2015).
111. Bakharev, P. V. et al. Chemically induced transformation of chemical vapour deposition grown bilayer graphene into fluorinated single-layer diamond. *Nat. Nanotechnol.* **15**, 59–66 (2020).
112. Gleason, K. K. Nanoscale control by chemically vapour-deposited polymers. *Nat. Rev. Phys.* **2**, 347–364 (2020).
This review introduces the controllable growth of polymers via CVD.
113. Zhan, Y., Liu, Z., Najmaei, S., Ajayan, P. M. & Lou, J. Large-area vapor-phase growth and characterization of MoS_2 atomic layers on a SiO_2 substrate. *Small* **8**, 966–971 (2012).
114. Chhowalla, M., Liu, Z. & Zhang, H. Two-dimensional transition metal dichalcogenide (TMD) nanosheets. *Chem. Soc. Rev.* **44**, 2584–2586 (2015).
This review article introduces 2D TMDs.
115. Lv, R. et al. Transition metal dichalcogenides and beyond: synthesis, properties, and applications of single- and few-layer nanosheets. *Acc. Chem. Res.* **48**, 56–64 (2015).
116. Liu, K.-K. et al. Growth of large-area and highly crystalline MoS_2 thin layers on insulating substrates. *Nano Lett.* **12**, 1538–1544 (2012).
117. Wang, X. et al. Chemical vapor deposition growth of crystalline monolayer $MoSe_2$. *ACS Nano* **8**, 5125–5131 (2014).
118. Huang, C. et al. Lateral heterojunctions within monolayer $MoSe_2$–WSe_2 semiconductors. *Nat. Mater.* **13**, 1096–1101 (2014).
119. Liu, B. et al. Chemical vapor deposition growth of monolayer WSe_2 with tunable device characteristics and growth mechanism study. *ACS Nano* **9**, 6119–6127 (2015).
120. Li, S. et al. Halide-assisted atmospheric pressure growth of large WSe_2 and WS_2 monolayer crystals. *Appl. Mater. Today* **1**, 60–66 (2015).
121. Li, G. et al. Direct growth of continuous and uniform MoS_2 film on SiO_2/Si substrate catalyzed by sodium sulfate. *J. Phys. Chem. Lett.* **11**, 1570–1577 (2020).
122. Yang, P. et al. Batch production of 6-inch uniform monolayer molybdenum disulfide catalyzed by sodium in glass. *Nat. Commun.* **9**, 979 (2018).
123. Lee, Y.-H. et al. Synthesis of large-area MoS_2 atomic layers with chemical vapor deposition. *Adv. Mater.* **24**, 2320–2325 (2012).
124. Dumcenco, D. et al. Large-area epitaxial monolayer MoS_2. *ACS Nano* **9**, 4611–4620 (2015).
125. Kang, K. et al. High-mobility three-atom-thick semiconducting films with wafer-scale homogeneity. *Nature* **520**, 656–660 (2015).
126. Kim, H., Ovchinnikov, D., Deiana, D., Unuchek, D. & Kis, A. Suppressing nucleation in metal–organic chemical vapor deposition of MoS_2 monolayers by alkali metal halides. *Nano Lett.* **17**, 5056–5063 (2017).
127. Xu, C. et al. Large-area high-quality 2D ultrathin Mo_2C superconducting crystals. *Nat. Mater.* **14**, 1135–1141 (2015).
128. Wang, Y. et al. Van der Waals contacts between three-dimensional metals and two-dimensional semiconductors. *Nature* **568**, 70–74 (2019).
129. Zhou, J. et al. A library of atomically thin metal chalcogenides. *Nature* **556**, 355–359 (2018).
130. Yang, J. et al. Ultrahigh-current-density niobium disulfide catalysts for hydrogen evolution. *Nat. Mater.* **18**, 1309–1314 (2019).
131. Behura, S., Nguyen, P., Che, S., Debbarma, R. & Berry, V. Large-area, transfer-free, oxide-assisted synthesis of hexagonal boron nitride films and their heterostructures with MoS_2 and WS_2. *J. Am. Chem. Soc.* **137**, 13060–13065 (2015).
132. Wang, L. et al. Epitaxial growth of a 100-square-centimetre single-crystal hexagonal boron nitride monolayer on copper. *Nature* **570**, 91–95 (2019).
133. Wang, Z. et al. Metal immiscibility route to synthesis of ultrathin carbides, borides, and nitrides. *Adv. Mater.* **29**, e1700364 (2017).
134. Wu, J. et al. High electron mobility and quantum oscillations in non-encapsulated ultrathin semiconducting Bi_2O_2Se. *Nat. Nanotechnol.* **12**, 530–534 (2017).
135. Tan, C. et al. Wafer-scale growth of single-crystal 2D semiconductor on perovskite oxides for high-performance transistors. *Nano Lett.* **19**, 2148–2153 (2019).
136. Gleason, K. K. *CVD Polymers: Fabrication of Organic Surfaces and Devices* (Wiley, 2015).
137. De Luna, M. M., Karandikar, P. & Gupta, M. Interactions between polymers and liquids during initiated chemical vapor deposition onto liquid substrates. *Mol. Syst. Des. Eng.* **5**, 15–21 (2020).
138. Donadt, T. B. & Yang, R. Vapor-deposited biointerfaces and bacteria: an evolving conversation. *ACS Biomater. Sci. Eng.* **6**, 182–197 (2020).
139. Moni, P., Al-Obeidi, A. & Gleason, K. K. Vapor deposition routes to conformal polymer thin films. *Beilstein J. Nanotechnol.* **8**, 723–735 (2017).
140. Coclite, A. M. Smart surfaces by initiated chemical vapor deposition. *Surf. Innov.* **1**, 6–14 (2013).
141. Gleason, K. K. Chemically vapor deposited polymer nanolayers for rapid and controlled permeation of molecules and ions. *J. Vac. Sci. Technol.* **38**, 020801 (2020).
142. Perrotta, A., Werzer, O. & Coclite, A. M. Strategies for drug encapsulation and controlled delivery based on vapor-phase deposited thin films. *Adv. Eng. Mater.* **20**, 1700639 (2018).
143. Sayin, S., Ozdemir, E., Acar, E. & Ince, G. O. Multifunctional one-dimensional polymeric nanostructures for drug delivery and biosensor applications. *Nanotechnology* **30**, 412001 (2019).
144. Zhao, J. & Gleason, K. K. Solvent-less vapor-phase fabrication of membranes for sustainable separation processes. *Engineering* https://doi.org/10.1016/j.eng.2020.05.002 (2020).
145. Lewis, H. G. P., Bansal, N. P., White, A. J. & Handy, E. S. HWCVD of polymers: commercialization and scale-up. *Thin Solid Films* **517**, 3551–3554 (2009).
146. Kim, S. et al. Ultrathin high-resolution flexographic printing using nanoporous stamps. *Sci. Adv.* **2**, e1601660 (2016).
147. Suh, H. S. et al. Sub-10-nm patterning via directed self-assembly of block copolymer films with a vapour-phase deposited topcoat. *Nat. Nanotechnol.* **12**, 575 (2017).
148. Moni, P. et al. Ultrathin and conformal initiated chemical-vapor-deposited layers of systematically varied surface energy for controlling the directed self-assembly of block copolymers. *Langmuir* **34**, 4494–4502 (2018).
149. Yang, G. G. et al. Conformal 3D nanopatterning by block copolymer lithography with vapor-phase deposited neutral adlayer. *ACS Nano* **13**, 13092–13099 (2019).
150. Yu, S. J. et al. Initiated chemical vapor deposition: a versatile tool for various device applications. *Adv. Eng. Mater.* **20**, 1700622 (2018).
This review article highlights the synthesis of polymers via an advanced CVD method.
151. Kim, J. H. et al. Conformal, wafer-scale and controlled nanoscale doping of semiconductors via the iCVD process. *IEEE Int. Electron Devices Meet.* https://doi.org/10.1109/IEDM.2018.8614494 (2018).
152. Gharahcheshmeh, M. H. & Gleason, K. K. Device fabrication based on oxidative chemical vapor deposition (oCVD) synthesis of conducting polymers and related conjugated organic materials. *Adv. Mater. Interfaces* **6**, 1801564 (2019).
153. Wang, X. et al. High electrical conductivity and carrier mobility in oCVD PEDOT thin films by engineered crystallization and acid treatment. *Sci. Adv.* **4**, eaat5780 (2018).
This paper shows that the electrical conductivity and carrier mobility of a mechanically flexible CVD organic polymer thin film reaches the levels found in mechanical brittle ITO.
154. Gueye, M. N., Carella, A., Faure-Vincent, J., Demadrille, R. & Simonato, J.-P. Progress in understanding structure and transport properties of PEDOT-based materials: a critical review. *Prog. Mater. Sci.* **108**, 100616 (2019).
155. Smolin, Y. Y., Soroush, M. & Lau, K. K. Influence of oCVD polyaniline film chemistry in carbon-based supercapacitors. *Ind. Eng. Chem. Res.* **56**, 6221–6228 (2017).
156. Lau, K. K. & Gleason, K. K. Initiated chemical vapor deposition (iCVD) of poly(alkyl acrylates): an experimental study. *Macromolecules* **39**, 3688–3694 (2006).
157. Tao, R. & Anthamatten, M. Condensation and polymerization of supersaturated monomer vapor. *Langmuir* **28**, 16580–16587 (2012).
158. O'Shaughnessy, W., Murthy, S., Edell, D. & Gleason, K. Stable biopassive insulation synthesized by initiated chemical vapor deposition of poly (1,3,5-trivinyltrimethylcyclotrisiloxane). *Biomacromolecules* **8**, 2564–2570 (2007).
159. Obraztsov, A. N., Obraztsova, E. A., Tyurnina, A. V. & Zolotukhin, A. A. Chemical vapor deposition of thin graphite films of nanometer thickness. *Carbon* **45**, 2017–2021 (2007).
160. Yu, Q. et al. Graphene segregated on Ni surfaces and transferred to insulators. *Appl. Phys. Lett.* **93**, 113103 (2008).
161. Lee, Y. et al. Wafer-scale synthesis and transfer of graphene films. *Nano Lett.* **10**, 490–493 (2010).
162. Hong, B. H. et al. Graphene roll-to-roll coating apparatus and graphene roll-to-roll coating method using the same. US KR1020100011437 patent (2010).
163. Han, T.-H. et al. Extremely efficient flexible organic light-emitting diodes with modified graphene anode. *Nat. Photonics* **6**, 105–110 (2012).
164. Kang, J. et al. High-performance graphene-based transparent flexible heaters. *Nano Lett.* **11**, 5154–5158 (2011).
165. Kang, S. et al. Efficient heat generation in large-area graphene films by electromagnetic wave absorption. *2D Mater.* **4**, 025037 (2017).
166. Kobayashi, T. et al. Production of a 100-m-long high-quality graphene transparent conductive film by roll-to-roll chemical vapor deposition and transfer process. *Appl. Phys. Lett.* **102**, 023112 (2013).
167. Hesjedal, T. Continuous roll-to-roll growth of graphene films by chemical vapor deposition. *Appl. Phys. Lett.* **98**, 133106 (2011).
168. Zhong, G. et al. Growth of continuous graphene by open roll-to-roll chemical vapor deposition. *Appl. Phys. Lett.* **109**, 193103 (2016).
169. Polsen, E. S., McNerny, D. Q., Viswanath, B., Pattinson, S. W. & John Hart, A. High-speed roll-to-roll manufacturing of graphene using a concentric tube CVD reactor. *Sci. Rep.* **5**, 10257 (2015).
170. Kim, D. J. E. A. Confocal laser scanning microscopy as a real time quality-assessment tool for industrial graphene synthesis. *2D Mater.* **7**, 045014 (2020).
171. Hong, B. H. Commercial scale production of CVD graphene and graphene quantum dots. Presented at Graphene and 2DM Industrial Forum (2020).
172. Robertson, J., Liu, X., Yue, C., Escarra, M. & Wei, J. Wafer-scale synthesis of monolayer and few-layer MoS_2 via thermal vapor sulfurization. *2D Mater.* **4**, 045007 (2017).

173. Lim, Y. R. et al. Roll-to-roll production of layer-controlled molybdenum disulfide: a platform for 2D semiconductor-based industrial applications. *Adv. Mater.* **30**, 1705270 (2018).
174. Hempel, M. et al. Repeated roll-to-roll transfer of two-dimensional materials by electrochemical delamination. *Nanoscale* **10**, 5522–5531 (2018).
175. Jeon, W., Cho, Y., Jo, S., Ahn, J.-H. & Jeong, S.-J. Wafer-scale synthesis of reliable high-mobility molybdenum disulfide thin films via inhibitor-utilizing atomic layer deposition. *Adv. Mater.* **29**, 1703031 (2017).
176. Choi, T. et al. Roll-to-roll continuous patterning and transfer of graphene via dispersive adhesion. *Nanoscale* **7**, 7138–7142 (2015).
177. Jo, I. et al. Tension-controlled single-crystallization of copper foils for roll-to-roll synthesis of high-quality graphene films. *2D Mater.* **5**, 024002 (2018).
178. Jin, S. et al. Colossal grain growth yields single-crystal metal foils by contact-free annealing. *Science* **362**, 1021 (2018).
179. Lee, J. S. et al. Wafer-scale single-crystal hexagonal boron nitride film via self-collimated grain formation. *Science* **362**, 817 (2018).
180. Kim, Y.-J., Kim, Y., Novoselov, K. & Hong, B. H. Engineering electrical properties of graphene: chemical approaches. *2D Mater.* **2**, 042001 (2015).
181. Zhao, L. et al. Visualizing individual nitrogen dopants in monolayer graphene. *Science* **333**, 999 (2011).
182. Kim, Y. et al. Vapor-phase molecular doping of graphene for high-performance transparent electrodes. *ACS Nano* **8**, 868–874 (2014).
183. Kim, Y. et al. A highly conducting graphene film with dual-side molecular n-doping. *Nanoscale* **6**, 9545–9549 (2014).
184. Jo, I. et al. Stable n-type doping of graphene via high-molecular-weight ethylene amines. *Phys. Chem. Chem. Phys.* **17**, 29492–29495 (2015).
185. Yan, C. et al. Mechanical and environmental stability of polymer thin-film-coated graphene. *ACS Nano* **6**, 2096–2103 (2012).
186. Choi, K. et al. Reduced water vapor transmission rate of graphene gas barrier films for flexible organic field-effect transistors. *ACS Nano* **9**, 5818–5824 (2015).
187. Kim, D. J. et al. Degradation protection of color dyes encapsulated by graphene barrier films. *Chem. Mater.* **31**, 7173–7177 (2019).
188. Kim, J. et al. Low-temperature synthesis of large-area graphene-based transparent conductive films using surface wave plasma chemical vapor deposition. *Appl. Phys. Lett.* **98**, 091502 (2011).
189. Havener, R. W. et al. High-throughput graphene imaging on arbitrary substrates with widefield Raman spectroscopy. *ACS Nano* **6**, 373–380 (2012).
190. Krupka, J., Strupinski, W. & Kwietniewski, N. Microwave conductivity of very thin graphene and metal films. *J. Nanosci. Nanotechnol.* **11**, 3358–3362 (2011).
191. Whelan, P. R. et al. Robust mapping of electrical properties of graphene from terahertz time-domain spectroscopy with timing jitter correction. *Opt. Express* **25**, 2725–2732 (2017).
192. Panchal, V. et al. Confocal laser scanning microscopy for rapid optical characterization of graphene. *Commun. Phys.* **1**, 83 (2018).
193. Ci, L. et al. Preparation of carbon nanofibers by the floating catalyst method. *Carbon* **38**, 1933–1937 (2000).
194. Wang, B. W. et al. Continuous fabrication of meter-scale single-wall carbon nanotube films and their use in flexible and transparent integrated circuits. *Adv. Mater.* **30**, e1802057 (2018).
195. Huang, J.-K. et al. Large-area synthesis of highly crystalline WSe_2 monolayers and device applications. *ACS Nano* **8**, 923–930 (2014).
196. Geng, D. et al. Direct synthesis of large-area 2D Mo_2C on in situ grown graphene. *Adv. Mater.* **29**, 1700072 (2017).
197. Coclite, A. M. et al. 25th Anniversary article: CVD polymers: a new paradigm for surface modifi cation and device fabrication. *Adv. Mater.* **25**, 5392–5423 (2013).
198. Zhou, H. & Bent, S. F. Fabrication of organic interfacial layers by molecular layer deposition: present status and future opportunities. *J. Vac. Sci. Technol.* **31**, 040801 (2013).
199. George, S. M., Yoon, B. & Dameron, A. A. Surface chemistry for molecular layer deposition of organic and hybrid organic–inorganic polymers. *Acc. Chem. Res.* **42**, 498–508 (2009).
200. Bilger, D., Homayounfar, S. Z. & Andrew, T. L. A critical review of reactive vapor deposition for conjugated polymer synthesis. *J. Mater. Chem. C* **7**, 7159–7174 (2019).
201. Gharahcheshmeh, M. H. & Gleason, K. K. Engineering texture and nanostrcuture in conjugated conducting and semiconducting polymers. *Mater. Today Adv.* **8**, 100086 (2020).
202. Chen, H.-Y. & Lahann, J. Designable biointerfaces using vapor-based reactive polymers. *Langmuir* **27**, 34–48 (2011).
203. Hassan, Z., Spuling, E., Knoll, D. M. & Bräse, S. Regioselective functionalization of [2.2]paracyclophanes: recent synthetic progress and perspectives. *Angew. Chem. Int. Ed.* **59**, 2156–2170 (2020).
204. Yasuda, H. K. *Plasma Polymerization* (Academic, 1985).
205. van der Zande, A. M. et al. Grains and grain boundaries in highly crystalline monolayer molybdenum disulphide. *Nat. Mater.* **12**, 554–561 (2013).
206. Kovacik, P., del Hierro, G., Livernois, W. & Gleason, K. K. Scale-up of oCVD: large-area conductive polymer thin films for next-generation electronics. *Mater. Horiz.* **2**, 221–227 (2015).
207. Barr, M. C. et al. Direct monolithic integration of organic photovoltaic circuits on unmodified paper. *Adv. Mater.* **23**, 3500–3505 (2011).
208. Lau, K. K. et al. Superhydrophobic carbon nanotube forests. *Nano Lett.* **3**, 1701–1705 (2003).
209. Yang, S. C. et al. Large-scale, low-power nonvolatile memory based on few-layer MoS_2 and ultrathin polymer dielectrics. *Adv. Electron. Mater.* **5**, 1800688 (2019).

Acknowledgements
Z.F.L. and L.Z.S. were supported by Beijing National Laboratory for Molecular Sciences (BNLMS-CXTD-202001), Beijing Municipal Science & Technology Commission (Nos. Z181100004818001 and Z191100000819005), the National Basic Research Program of China (No. 2016YFA0200101) and the National Natural Science Foundation of China (Nos. 21525310, 51432002 and 51520105003). B.H.H. acknowledges D. J. Kim, Graphene Square Inc., for the illustration in Figs 8, 9a and 10a.

Author contributions
Introduction (Z.F.L and L.Z.S); Experimentation (Z.F.L. and L.Z.S.); Results (L.B.G. and G.W.Y.); Applications (M.C., J.E.Y., K.K.G., M.H.G., B.H.H. and Y.S.C.); Reproducibility and data deposition (B.H.H. and Y.S.C.); Outlook (M.C. and J.E.Y.); Overview of Primer (Z.F.L.). All authors discussed and edited the full manuscript.

Competing interests
K.K.G is a co-founder of GVD Corporation and DropWise Technologies. Both companies are commercializing CVD polymerization.

Peer review information
Nature Reviews Methods Primers thanks J.H. Ahn, G. İnce, T. Kobayashi, A.N. Obraztsov, F. Stadler and the other, anonymous, reviewer(s) for their contribution to the peer review of this work.

Publisher's note
Springer Nature remains neutral with regard to jurisdictional claims in published maps and institutional affiliations.